Advances in Water Resources 142 (2020) 103604

Contents lists available at ScienceDirect

Advances in Water Resources

journal homepage: www.elsevier.com/locate/advwatres

# Transient flow to a finite-radius well with wellbore storage and skin effect in a poroelastic confined aquifer

Zhiqiang Fan*, Rishi Parashar

*Division of Hydrologic Sciences, Desert Research Institute, Reno, NV, 89512, USA*

ARTICLE INFO

*Keywords:*
Poroelasticity
Wellbore skin
Wellbore storage
Pumping test
Confined aquifer

ABSTRACT

This paper presents analytical solutions for pumping from a poroelastic, confined aquifer where the combined effects of a finite-thickness skin zone and the wellbore storage are fully incorporated. The pumping-induced axisymmetric stress, plane strain deformation, and pore pressure are derived in the Laplace transform domain. Time-domain solutions are obtained using the Stehfest inversion algorithm. Numerical examples are presented to investigate the effects of hydromechanical coupling and poroelasticity on the hydraulic drawdown at the pumping well and at an observation well. The results show that traditional methods substantially underestimate the drawdown at the pumping well in a low-permeability hard rock compared with the drawdown predicted using the fully coupled poroelastic theory. The difference becomes more pronounced when a finite-thickness positive skin is present with a permeability that is lower than the permeability of the formation. For finite-radius pumping wells with storage, the effects of poroelasticity on drawdown are masked by the effects associated with wellbore storage.

## 1. Introduction

Pumping tests in confined aquifers are widely used to estimate hydraulic properties (e.g., hydraulic conductivity and specific storage) of aquifers for a wide range of applications from groundwater extraction to potential site evaluation for nuclear-waste disposal. A pumping test typically involves pumping a well at a carefully controlled rate for a period to create a measurable pressure perturbation in the formation, and to measure the rate of flow at the well and the drawdown in observation wells located at different distances from the pumping well (Yeh and Chang, 2013). Interpretation and analysis of the drawdown data collected during a pumping test is largely based on fitting type curves generated from available analytical solutions. Since the seminal work by Theis (1935)—which produced an analytical solution for drawdown induced by a fully penetrating well of infinitesimal radius pumping water at a constant rate from an infinite homogeneous confined aquifer—a variety of analytical solutions have been developed to address pumping tests under different well and aquifer configurations (Chen, 1984; Cassiani et al., 1999; Chang and Chen, 2002; Yang et al., 2006; Yeh and Chang, 2013;). In particular, several researchers have focused on the effects of a finite well radius (Moench, 1997; Yang et al., 2006), wellbore storage (Park and Zhan, 2002; Razminia et al., 2016; Li et al., 2018), the skin zone (Chang and Chen, 2002; Pasandi et al., 2008; Razminia et al., 2015; Feng and Zhan, 2016), and the permeability anisotropy (Mathias and Butler, 2007) on transient flow behavior. For example, Hantush (1964) developed an analytical solution for constant-rate pumping in confined aquifers by taking into consideration the effects of a finite well radius. Papadopulos and Cooper (1967) extended the Hantush (1964) solution by accounting for wellbore storage for a fully penetrating well. In addition to the storage and radius of the pumping well, the induced drawdown at a control well can also be strongly influenced by a skin zone, which is conceptualized as the surrounding zone of a well with reduced/enhanced permeability resulting from drilling or completion operations (Yeh and Chang, 2013). A negative/positive skin refers to a skin zone with a permeability that is larger/smaller than the permeability of the formation zone. In petroleum engineering applications, wellbore skin factors are commonly introduced to quantify the skin effect on fluid flow without modeling skin zone explicitly (Dejam et al., 2013). The nondimensional skin factor is defined as (Yeh and Chang, 2013):

$$s_f = \left[K_2/K_1 - 1\right] \ln\left(r_S/r_W\right) \tag{1}$$

where $K_2$ and $K_1$ are the hydraulic conductivities of the formation and skin zone, respectively, and $r_S$ and $r_W$ are the skin zone radius and wellbore radius (measured from the axis of the well), respectively. According to Novakowski (1989), the thickness (i.e., the difference between $r_S$ and $r_W$) of the skin zone may range from a few millimeters to sev-

* Corresponding author.
*E-mail address:* kuangshiqicai@gmail.com (Z. Fan).

https://doi.org/10.1016/j.advwatres.2020.103604
Received 30 September 2019; Received in revised form 26 April 2020; Accepted 26 April 2020
Available online 20 May 2020

**Nomenclature**

| | |
|---|---|
| $\alpha$ | Biot coefficient |
| $\varepsilon_{rr}$ | radial strain |
| $\varepsilon_{kk}$ | bulk strain |
| $\zeta$ | increment of fluid content |
| $\mu_f$ | pore fluid viscosity ($ML^{-1}T^{-1}$) |
| $\nu_u$ | undrained Poisson's ratio |
| $\sigma_{ij}$ | total stress ($M\,L^{-1}\,T^{-2}$) |
| $\sigma_{rr}$ | radial stress ($M\,L^{-1}\,T^{-2}$) |
| $\sigma_{zz}$ | axial stress ($M\,L^{-1}\,T^{-2}$) |
| $c$ | hydraulic diffusivity ($L^2\,T^{-1}$) |
| $p$ | excess pore pressure ($M\,L^{-1}\,T^{-2}$) |
| $r$ | radial distance from the axis of the pumping well (L) |
| $r_S$ | radius of skin zone (L) |
| $s_h$ | hydraulic drawdown (L) |
| $u_r$ | radial displacement (L) |
| $C_W$ | wellbore storage coefficient ($L^2$) |
| $G$ | shear modulus ($M\,L^{-1}\,T^{-2}$) |
| $I_0$ | modified Bessel function of the first kind of order zero |
| $K_1$ | modified Bessel function of second kind of first order |
| $K_f$ | bulk modulus of fluid ($M\,L^{-1}\,T^{-2}$) |
| $K_V$ | drained vertical bulk modulus ($M\,L^{-1}\,T^{-2}$) |
| $N$ | total number of terms in the Stehfest series |
| $Q$ | volumetric pumping rate ($L^3T^{-1}$) |

*Superscript*

| | |
|---|---|
| $*$ | dimensionless variable |
| $\varepsilon_{ij}$ | strain components |
| $\varepsilon_{\theta\theta}$ | hoop strain |
| $\varepsilon_{zz}$ | axial strain |
| $\kappa$ | mobility ($M^{-1}\,L^3\,T$) |
| $\nu$ | drained Poisson's ratio |
| $\rho_f$ | mass density of the fluid ($M\,L^{-3}$) |
| $\sigma_{kk}$ | bulk stress ($M\,L^{-1}\,T^{-2}$) |
| $\sigma_{\theta\theta}$ | hoop stress ($M\,L^{-1}\,T^{-2}$) |
| $\phi$ | porosity |
| $k$ | intrinsic permeability ($L^2$) |
| $p_w$ | pressure at the wellbore ($M\,L^{-1}\,T^{-2}$) |
| $r_C$ | radius of well casing (L) |
| $r_W$ | radius of pumping well (L) |
| $s$ | Laplace transform variable |
| $t$ | time (T) |
| $B$ | Skempton's coefficient |
| $E$ | Young's modulus ($M\,L^{-1}\,T^{-2}$) |
| $H$(t) | Heaviside function |
| $I_1$ | modified Bessel function of the first kind of first order |
| $K_0$ | modified Bessel function of second kind of order zero |
| $K_b$ | bulk modulus of fluid-saturated rock ($M\,L^{-1}\,T^{-2}$) |
| $K_s$ | bulk modulus of solid ($M\,L^{-1}\,T^{-2}$) |
| $M$ | Biot modulus ($M\,L^{-1}\,T^{-2}$) |
| $S_s$ | specific storage ($L^{-1}$) |

*Subscript*

| | |
|---|---|
| 1,2 | skin zone, formation zone |

eral meters. Skin zones that develop during the well drilling because of drilling mud and/or rock flour invasion have lower permeability than the formation and are defined as a positive skin. Conversely, negative skin zones with permeability higher than the formation develop when the drilling method induces substantial spalling and fracturing of the borehole wall. Butler (1988) investigated the problem of a well of infinitesimal radius with a finite-thickness skin zone subject to a constant-rate pumping by treating the well as a point force and found that the drawdown during a pumping test can be considered to consist of two components that are dependent and independent of near-well properties. Novakowski (1989) solved the problem of a fully penetrating well subjected to a constant-rate pumping in a confined aquifer, accounting simultaneously for finite wellbore radius, finite-thickness skin zone, and wellbore storage. Yeh et al. (2003) derived the closed-form time-domain solution of the drawdown for a pumping test in a confined aquifer in terms of an improper integral, which included the effects of a finite wellbore radius and finite-thickness skin zone. By accounting for the wellbore storage effect and the skin effect using the lumped skin factor (Eq. (1)), Dejam et al. (2013) investigated the behavior of transient pressure at a partially penetrating well in a naturally fractured reservoir and applied it to generate type curves to analyze the pressure of wellbores with a gas cap. Razminia et al. (2016) examined the transient pressure in a fractal reservoir by taking into consideration both the wellbore storage and skin effects.

The aforementioned solutions were all developed using the traditional groundwater flow conceptual model, which does not include the poroelastic effects associated with a pumping test. The pumping-induced horizontal deformation of an aquifer is well documented and recognized (Hsieh and Cooley, 1995; Hsieh, 1996; Berg et al., 2011; Burbey, 1999, 2003; Yin et al., 2007; Sneed et al., 2018), but it remains a common assumption in groundwater theory that solid grains are incompressible and horizontal deformation of an aquifer is thought to have a negligible effect on pressure transience (Wang, 2000; De Simone and Carrera, 2017; Fan et al., 2019). Although computed values of the hydraulic properties of aquifers using models based on groundwater flow theory yield significant insights into the physics controlling the feedback and interaction between well parameters and aquifer configurations, using traditional models to interpret pumping tests can lead to erroneous outcomes for cases with strong poroelastic effects (Berg et al., 2011; Ding et al., 2019; Fan et al., 2016, 2020; Fan and Parashar, 2019). Poroelastic effects are thought to play a prominent role in low-permeability hard rocks, which are systems of interest for a variety of applications in subsurface hydrogeology, such as nuclear waste storage (Tsang et al., 2015; Belmokhtar et al., 2016), enhanced geothermal systems (Koh et al., 2011; Ghassemi and Zhou, 2011; Fan and Parashar, 2019), and geological carbon sequestration (Wu et al., 2010; De Simone and Carrera, 2017). Accurate and reliable hydraulic characterization of low-permeability hard rocks is essential for assessing its long-term performance for various applications (Tsang et al., 2015). Strong hydromechanical coupling occurs in these rocks when the system is subjected to high pumping rates, and therefore taking into account the poroelastic effect may help obtain more accurate estimates of the subsurface properties.

The poroelastic effect for a well under a constant rate of discharge has been studied more extensively in petroleum engineering than in hydrology. For instance, Cheng (2016) presented the analytical solution for fluid extraction from a poroelastic reservoir at a constant rate. Abousleiman and Chen (2010) derived the poroelastic solution for an inclined borehole subjected to a finite-length fluid flux. Mehrabian and Abousleiman (2013) developed the fundamental poroelastic solutions for a wellbore under partial angular fluid flux and normal tractions. Chen (2019) further extended the solution of Abousleiman and Chen (2010) by developing three-dimensional analytical solutions for an arbitrarily inclined wellbore subjected to a fluid discharge of finite-length. These analytical poroelastic solutions (Abousleiman and Chen, 2010; Mehrabian and Abousleiman, 2013; Cheng, 2016; Chen, 2019) addressed the hydromechanical coupling associated with wells pumping at a constant rate, without accounting for the effects of skin zone and wellbore storage. To the best knowledge of the authors, analytical solutions accounting for poroelastic effects in a system with a finite radius well that consider the wellbore storage and skin zone effects have not yet been reported. The purpose of this paper is threefold: (1) to derive new analytical solutions for a pumping test that simultaneously accounts for poroelastic effect, wellbore storage, and finite wellbore skin zone; (2) to compare this new solution with transient

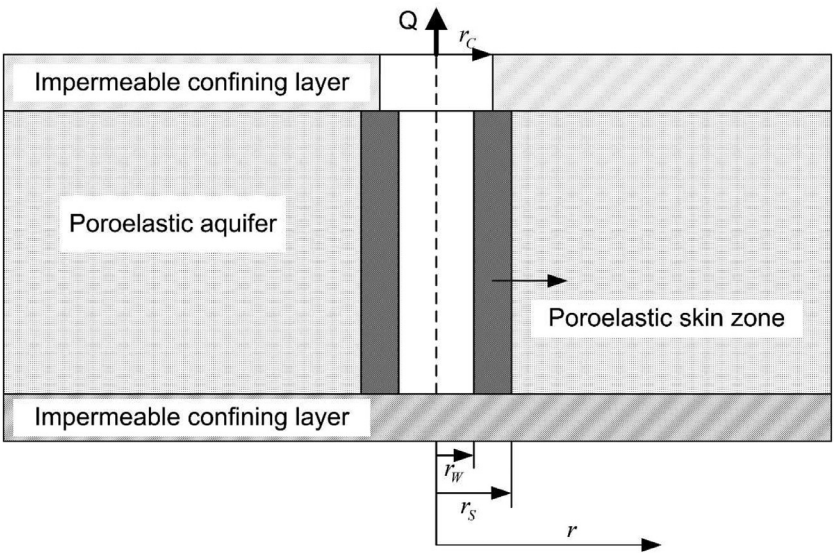


**Fig. 1.** Schematic illustration of a well subjected to a constant-rate pumping in a poroelastic confined aquifer.

solutions obtained from existing simpler analytical methods; and (3) to determine the conditions under which the drawdown solutions obtained are reasonably accurate and reliable without incorporating the poroelastic effect. We used Laplace transform to solve the governing equations in plane strain poroelasticity and explored the effects of wellbore storage, skin zone types/thickness, and poroelastic deformation on the temporal-spatial evolution of drawdown in the pumping well and in the aquifer. The results presented in this paper are expected to provide useful guidance for observation well placement and to help practitioners better interpret the pumping test results. The analytical solutions derived in this paper may serve as a benchmark for validating numerical models and methods in poroelasticity.

## 2. Mathematical formulation

### 2.1. Statement of the problem

Consider a fully penetrating pumping well of radius $r_W$ with a skin zone of radius $r_S$ embedded in a homogeneous, isotropic, poroelastic confined aquifer (Fig. 1). At time zero, pumping starts at a constant volumetric rate, $Q$, from the pumping well.

The key assumptions underlying the poroelastic formulation for the aforementioned system are as follows: (1) the aquifer is homogeneous and isotropic; (2) the pumped aquifer is horizontal and of infinite extent; (3) the aquifer is poroelastic and follows the classical Biot theory; (4) the skin zone and the formation have the same mechanical properties, but different hydraulic properties; and (5) the screen interval of the pumping well spans the thickness of the aquifer and the plane strain condition prevails in the horizontal plane. Within the classical framework of Biot poroelasticity, fluid flow is assumed to follow Darcy's law (Wang, 2000). We note that this simplified assumption may not be valid in ultra-tight, low-permeability media, particularly when the hydraulic gradient is very small (Neuzil, 1986; Dejam et al., 2017). The fourth assumption is justified based on observations that the skin zones develop mainly due to drilling and completion practices, which result in an altered permeability in a region surrounding a wellbore without significant changes in the mechanical properties (Nowakowski, 1989). Because the length of the screen interval of the pumping well is much larger than the well diameter, and the flux and traction boundary conditions do not vary along the wellbore axis, the plain strain condition is assumed.

For the plain strain condition, the constitutive equations in polar coordinate systems, which express the total stresses, $\sigma_{ij}$, and pore pressure, $p$, in terms of strains, $\varepsilon_{ij}$, and increment of fluid content, $\zeta$, are as follows (Wang, 2000; Cheng 2016):

$$\sigma_{rr} = 2G\varepsilon_{rr} + \frac{2G\nu_u}{1-2\nu_u}\varepsilon_{kk} - \alpha M\zeta \tag{2}$$

$$\sigma_{\theta\theta} = 2G\varepsilon_{\theta\theta} + \frac{2G\nu_u}{1-2\nu_u}\varepsilon_{kk} - \alpha M\zeta \tag{3}$$

$$\sigma_{zz} = \frac{2G\nu_u}{1-2\nu_u}\varepsilon_{kk} - \alpha M\zeta \tag{4}$$

$$p = M\left(\zeta - \alpha\varepsilon_{kk}\right) \tag{5}$$

where $\sigma_{rr}$,$\sigma_{\theta\theta}$, and $\sigma_{zz}$ are the radial, hoop, and axial stresses, respectively; $\varepsilon_{rr}$,$\varepsilon_{\theta\theta}$, and $\varepsilon_{zz}$ are the radial, hoop, and axial strains, respectively; and $\varepsilon_{kk}$ is the bulk strain. The material constants given above are: the shear modulus, $G$; the undrained Poisson's ratio, $\nu_u$; the Biot coefficient, $\alpha$; and the Biot modulus, $M$. The Biot coefficient, $\alpha$, is a ratio signifying the fluid volume change induced by the bulk volume change under drained conditions (Wang, 2000). For the axial symmetry case, the strain components are related to the displacement by:

$$\varepsilon_{rr} = \frac{\partial u_r}{\partial r}, \varepsilon_{\theta\theta} = \frac{u_r}{r}, \varepsilon_{zz} = 0 \tag{6}$$

where $u_r$ is the radial displacement. The bulk strain is given by:

$$\varepsilon_{kk} = \frac{\partial u_r}{\partial r} + \frac{u_r}{r} = \frac{1}{r}\frac{\partial}{\partial r}\left(ru_r\right) \tag{7}$$

For a fully saturated rock without any fluid sources or sinks, the conservation of fluid mass yields:

$$\frac{\partial \zeta}{\partial t} = c\nabla^2\zeta \tag{8}$$

Equivalently, Eq. (8) can be written as (Green and Wang, 1990):

$$\frac{\partial}{\partial t}\left(p + \frac{B}{3}\sigma_{kk}\right) = c\nabla^2\left(p + \frac{B}{3}\sigma_{kk}\right) \tag{9}$$

In the above $B$ is the Skempton's coefficient, which is defined as the ratio of the induced pore pressure to the change of bulk stress under undrained conditions (Wang, 2000), $c$ is the hydraulic diffusivity, which is defined as $c = \frac{\rho_f g k}{\mu S_s}$, and $S_s$ is the specific storage given by (Green and Wang, 1990; Wang, 1993):

$$S_s = \rho_f g\left[\phi\left(\frac{1}{K_f} - \frac{1}{K_s}\right) + \frac{\alpha}{K_V}\left(1 + \frac{4G}{3K_s}\right)\right] \tag{10}$$

where $\rho_f$ is the fluid density; $g$ is the gravitational acceleration; $k$ is permeability; $\mu$ is the fluid dynamic viscosity; $\phi$ is the porosity; $K_f$ and

$K_s$ are the bulk modulus for fluids and solids, respectively; and $K_V$ is the drained vertical bulk modulus (Wang, 2000), which can be expressed in terms of the bulk modulus, $K_b$, and shear modulus, $G$, of the matrix as follows:

$$K_V = K_b + \frac{4}{3}G \tag{11}$$

The equilibrium equation, which describes the system under the influence of radial and hoop stresses, is given by:

$$\frac{\partial \sigma_{rr}}{\partial r} + \frac{\sigma_{rr} - \sigma_{\theta\theta}}{r} = 0 \tag{12}$$

Substituting the constitutive Eqs. (2-3) and strain-displacement relations (6) and (7) into the equilibrium Eq. (12) yields the governing equation for displacement:

$$\frac{2G(1-\nu_u)}{1-2\nu_u}\left(\frac{\partial^2 u_r}{\partial r^2} + \frac{1}{r}\frac{\partial u_r}{\partial r} - \frac{u_r}{r^2}\right) = \alpha M \frac{\partial \varsigma}{\partial r} \tag{13}$$

Eq. (13) can be rearranged into:

$$\frac{\partial \varepsilon_{kk}}{\partial r} = \frac{\alpha M(1-2\nu_u)}{2G(1-\nu_u)}\frac{\partial \varsigma}{\partial r} \tag{14}$$

The initial conditions that describe the system before the onset of pumping are expressed by equating the excess pore pressure, increment of fluid content, radial stress, and radial displacement to zero:

$$p_1(r,0) = p_2(r,0) = 0 \tag{15}$$

$$\varsigma_1(r,0) = \varsigma_2(r,0) = 0 \tag{16}$$

$$\sigma_{r1}(r,0) = \sigma_{r2}(r,0) = 0 \tag{17}$$

$$u_{r1}(r,0) = u_{r2}(r,0) = 0 \tag{18}$$

where the subscripts 1 and 2 refer to the skin zone ($r_W \le r \le r_S$) and the formation zone

($r_S \le r < \infty$), respectively.

The boundary conditions are specified below.

At the far field:

$$p_2(\infty,0) = 0, \varsigma_2(\infty,0) = 0, \sigma_{r2}(\infty,0) = 0, u_{r2}(\infty,0) = 0 \tag{19}$$

At the borehole surface:

$$\sigma_{r1}(r_W,t) = -p_1(r_W,t)H(\mathrm{t}) \tag{20}$$

$$2\pi r_W b\frac{k_1}{\mu}\left.\frac{\partial p_1}{\partial r}\right|_{r=r_W} - \frac{C_W}{\rho_f g}\left.\frac{\partial p_1}{\partial t}\right|_{r=r_W} = -QH(t) \tag{21}$$

where $H$(t) is the Heaviside function, $p_1$ is the time-dependent fluid pressure required to pump at a constant rate, $Q$, from the wellbore. This is an implicit initial-boundary value problem because $p_1$ is unknown a priori. The wellbore storage coefficient is $C_W = \pi r_C^2$ (Novakowski, 1989), where $r_C$ is the radius of the well casing.

At the interface between the skin and formation zone ($r = r_S$), the continuity of the pore pressure, fluid flux, radial displacement, and radial stress leads to:

$$p_1(r_S,t) = p_2(r_S,t) \tag{22}$$

$$\kappa_1\frac{\partial p_1}{\partial r}(r_S,t) = \kappa_2\frac{\partial p_2}{\partial r}(r_S,t) \tag{23}$$

$$u_{r1}(r_S,t) = u_{r2}(r_S,t) \tag{24}$$

$$\sigma_{r1}(r_S,t) = \sigma_{r2}(r_S,t) \tag{25}$$

In Eq. (23), $\kappa_1 = k_1/\mu$ and $\kappa_2 = k_2/\mu$ are the mobility of the skin zone and formation, respectively.

### 2.2. Analytical solutions in the Laplace domain

Analytical solutions were derived in the Laplace domain. Appendix A provides the detailed derivations. In the skin zone, the Laplace-domain solutions for pore pressure; radial, hoop, and axial stresses; and displacement are:

$$\tilde{p}_1 = \frac{1}{s}\frac{Q\mu}{2\pi r_w b k_1\sqrt{s/c_1}}\frac{\Psi_2 I_0\left(r\sqrt{s/c_1}\right) + \Psi_1 K_0\left(r\sqrt{s/c_1}\right)}{\Psi_1 K_1\left(r_w\sqrt{s/c_1}\right) - \Psi_2 I_1\left(r_w\sqrt{s/c_1}\right) + \Psi_3} \tag{26}$$

$$\tilde{\sigma}_{rr1} = \frac{1}{s}\frac{Q\mu}{2\pi r_w b k_1\sqrt{s/c_1}}\frac{2\eta\Psi_1 F_1/\left(r\sqrt{s/c_1}\right) + 2\eta\Psi_2 F_2/\left(r\sqrt{s/c_1}\right) - F_3 r_w^2/r^2}{\Psi_1 K_1\left(r_w\sqrt{s/c_1}\right) - \Psi_2 I_1\left(r_w\sqrt{s/c_1}\right) + \Psi_3} \tag{27}$$

$$\tilde{\sigma}_{\theta\theta 1} = \frac{1}{s}\frac{Q\mu}{2\pi r_w b k_1\sqrt{s/c_1}}\frac{-2\eta\Psi_1 F_1/\left(r\sqrt{s/c_1}\right) - 2\eta\Psi_2 F_2/\left(r\sqrt{s/c_1}\right) + F_3 r_w^2/r^2 - 2\eta F_4}{\Psi_1 K_1\left(r_w\sqrt{s/c_1}\right) - \Psi_2 I_1\left(r_w\sqrt{s/c_1}\right) + \Psi_3} \tag{28}$$

$$\tilde{\sigma}_{zz1} = -\frac{1}{s}\frac{Q\mu}{2\pi r_w b k_1\sqrt{s/c_1}}\frac{2\eta F_4}{\Psi_1 K_1\left(r_w\sqrt{s/c_1}\right) - \Psi_2 I_1\left(r_w\sqrt{s/c_1}\right) + \Psi_3} \tag{29}$$

$$\tilde{u}_{r1} = \frac{1}{Gs}\frac{Q\mu}{2\pi r_w b k_1\sqrt{s/c_1}}\frac{-\eta\Psi_1 F_1/\sqrt{s/c_1} - \eta\Psi_2 F_2/\sqrt{s/c_1} + F_3 r_w^2/(2r)}{\Psi_1 K_1\left(r_w\sqrt{s/c_1}\right) - \Psi_2 I_1\left(r_w\sqrt{s/c_1}\right) + \Psi_3} \tag{30}$$

where the tilde represents the Laplace transform; $s$ is the transform variable; $I_0$ and $I_1$ are the modified Bessel function of the first kind of order zero and first order, respectively; and $K_0$ and $K_1$ are the modified Bessel function of the second kind of order zero and first order, respectively. Functions $\Psi_1$,$\Psi_2$, and $\Psi_3$ are given by:

$$\Psi_1 = \frac{k_2}{k_1}\sqrt{\frac{c_1}{c_2}}I_0\left(r_s\sqrt{s/c_1}\right)K_1\left(r_s\sqrt{s/c_2}\right) + I_1\left(r_s\sqrt{s/c_1}\right)K_0\left(r_s\sqrt{s/c_2}\right) \tag{31}$$

$$\Psi_2 = K_1\left(r_s\sqrt{s/c_1}\right)K_0\left(r_s\sqrt{s/c_2}\right) - \frac{k_2}{k_1}\sqrt{\frac{c_1}{c_2}}K_0\left(r_s\sqrt{s/c_1}\right)K_1\left(r_s\sqrt{s/c_2}\right) \tag{32}$$

and:

$$\Psi_3 = \frac{C_w s}{2\pi r_w b\rho g k_1/\mu\sqrt{s/c_1}}\left[\Psi_2 I_0\left(r_w\sqrt{s/c_1}\right) + \Psi_1 K_0\left(r_w\sqrt{s/c_1}\right)\right] \tag{33}$$

Functions $F_1$ -$F_4$ are defined as:

$$F_1 = K_1\left(r\sqrt{s/c_1}\right) - \frac{r_w}{r}K_1\left(r_w\sqrt{s/c_1}\right) \tag{34}$$

$$F_2 = \frac{r_w}{r}I_1\left(r_w\sqrt{s/c_1}\right) - I_1\left(r\sqrt{s/c_1}\right) \tag{35}$$

$$F_3 = \Psi_2 I_0\left(r_w\sqrt{s/c_1}\right) + \Psi_1 K_0\left(r_w\sqrt{s/c_1}\right) \tag{36}$$

$$F_4 = \Psi_2 I_0\left(r\sqrt{s/c_1}\right) + \Psi_1 K_0\left(r\sqrt{s/c_1}\right) \tag{37}$$

In the formation zone, the Laplace domain solutions for pore pressure; radial, hoop, and axial stresses; and displacement are given by:

$$\tilde{p}_2 = \frac{1}{s}\frac{Q\mu}{2\pi r_w b k_1\sqrt{s/c_1}}\frac{K_0\left(r\sqrt{s/c_2}\right)\left[\Psi_2 I_0\left(r_s\sqrt{s/c_1}\right)+\Psi_1 K_0\left(r_s\sqrt{s/c_1}\right)\right]}{K_0\left(r_s\sqrt{s/c_2}\right)\left[\Psi_1 K_1\left(r_w\sqrt{s/c_1}\right)-\Psi_2 I_1\left(r_w\sqrt{s/c_1}\right)+\Psi_3\right]} \tag{38}$$

$$\tilde{\sigma}_{rr2} = \frac{1}{s}\frac{Q\mu}{2\pi r_w b k_1\sqrt{s/c_1}}\frac{1}{\Psi_1 K_1\left(r_w\sqrt{s/c_1}\right)-\Psi_2 I_1\left(r_w\sqrt{s/c_1}\right)+\Psi_3} \times\left[\frac{2\eta}{r\sqrt{s/c_2}}\frac{F_5F_8}{K_0\left(r_s\sqrt{s/c_2}\right)}+\frac{2\eta\Psi_2}{r\sqrt{s/c_1}}F_6+\frac{2\eta\Psi_1}{r\sqrt{s/c_1}}F_7-\frac{r_w^2}{r^2}F_3\right] \tag{39}$$

$$\tilde{\sigma}_{\theta\theta 2} = \frac{1}{s}\frac{Q\mu}{2\pi r_w b k_1\sqrt{s/c_1}}\frac{1}{\Psi_1 K_1\left(r_w\sqrt{s/c_1}\right)-\Psi_2 I_1\left(r_w\sqrt{s/c_1}\right)+\Psi_3} \times\left[\frac{r_w^2}{r^2}F_3-\frac{2\eta F_8\left(F_5+r\sqrt{s/c_2}K_0\left(r\sqrt{s/c_2}\right)\right)}{r\sqrt{s/c_2}K_0\left(r_s\sqrt{s/c_2}\right)}-\frac{2\eta\Psi_2}{r\sqrt{s/c_1}}F_6-\frac{2\eta\Psi_1}{r\sqrt{s/c_1}}F_7\right] \tag{40}$$

$$\tilde{\sigma}_{zz2} = -\frac{1}{s}\frac{Q\mu}{2\pi r_w b k_1\sqrt{s/c_1}}\frac{K_0\left(r\sqrt{s/c_2}\right)}{K_0\left(r_s\sqrt{s/c_2}\right)} \times\frac{2\eta F_8}{\Psi_1 K_1\left(r_w\sqrt{s/c_1}\right)-\Psi_2 I_1\left(r_w\sqrt{s/c_1}\right)+\Psi_3} \tag{41}$$

$$\tilde{u}_{r2} = \frac{1}{sG}\frac{Q\mu}{2\pi r_w b k_1\sqrt{s/c_1}}\frac{1}{\Psi_1 K_1\left(r_w\sqrt{s/c_1}\right)-\Psi_2 I_1\left(r_w\sqrt{s/c_1}\right)+\Psi_3} \times\left[\frac{r_w^2}{2r}F_3-\frac{\eta F_5F_8}{\sqrt{s/c_2}K_0\left(r_s\sqrt{s/c_2}\right)}-\frac{\eta}{\sqrt{s/c_1}}\Psi_2F_6-\frac{\eta}{\sqrt{s/c_1}}\Psi_1F_7\right] \tag{42}$$

where functions $F_5$ -$F_8$ are defined as:

$$F_5 = K_1\left(r\sqrt{s/c_2}\right)-\frac{r_s}{r}K_1\left(r_s\sqrt{s/c_2}\right) \tag{43}$$

$$F_6 = \frac{r_w}{r}I_1\left(r_w\sqrt{s/c_1}\right)-\frac{r_s}{r}I_1\left(r_s\sqrt{s/c_1}\right) \tag{44}$$

$$F_7 = \frac{r_s}{r}K_1\left(r_s\sqrt{s/c_1}\right)-\frac{r_w}{r}K_1\left(r_w\sqrt{s/c_1}\right) \tag{45}$$

$$F_8 = \Psi_2 I_0\left(r_s\sqrt{s/c_1}\right)+\Psi_1 K_0\left(r_s\sqrt{s/c_1}\right) \tag{46}$$

### 2.3. Dimensionless solutions

Dimensionless solutions were determined using the following nondimensional variables from Novakowski (1989) and Yeh et al. (2003):$c^* = c_2/c_1, k^* = k_2/k_1$, $C_W^* = C_W/(2\pi r_W^2 b S_{s2})$, $\rho = r/r_W$, $\rho_s = r_S/r_W$, $t^* = c_2 t/r_W^2, \beta = r_w\sqrt{s/c_2}$, $\xi = r\sqrt{s/c_2}$, $p^* = p(2\pi b\kappa_2)/Q, \sigma_{rr}^* = 2\pi b\kappa_2\sigma_{rr}/Q, \sigma_{\theta\theta}^* = 2\pi b\kappa_2\sigma_{\theta\theta}/Q, \sigma_{zz}^* = 2\pi b\kappa_2\sigma_{zz}/Q$, and $u_r^* = 2\pi G b\kappa_2 u_r/(Qr_W)$, where $t^*$ is the dimensionless time; $C_W^*$ is a dimensionless measure of the wellbore storage; $\rho$ is the dimensionless radial distance from the pumping well; $\rho_s$ is the dimensionless skin thickness; $\sigma_{rr}^*, \sigma_{\theta\theta}^*$, and $\sigma_{zz}^*$ are dimensionless radial, hoop, and axial stresses, respectively; $u_r^*$ is dimensionless radial displacement; and $p^*$ is dimensionless pore pressure change. The hydraulic drawdown, $s_h$, is related to the pore pressure drop, $p$, through:

$$s_h = \frac{p}{\rho_f g} \tag{47}$$

The dimensionless drawdown and its gradient are respectively defined as:

$$s_h^* = 2\pi b K_2 s_h/Q \tag{48}$$

$$s_{h,\rho}^* = \frac{\partial s_h^*}{\partial\rho} \tag{49}$$

The Laplace domain solutions for dimensionless variables, obtained by nondimensionalizing the solutions presented in the previous section, are given below.

In the skin zone:

$$\tilde{p}_1^* = \tilde{s}_{h1}^* = \frac{1}{s}\frac{k^*}{\beta\sqrt{c^*}}\frac{\Psi_2^* I_0\left(\rho\beta\sqrt{c^*}\right)+\Psi_1^* K_0\left(\rho\beta\sqrt{c^*}\right)}{\Psi_1^* K_1\left(\beta\sqrt{c^*}\right)-\Psi_2^* I_1\left(\beta\sqrt{c^*}\right)+\Psi_3^*} \tag{50}$$

$$\tilde{s}_{h1,\rho}^* = \frac{1}{s}\frac{k^*\left[\Psi_2^* I_1\left(\rho\beta\sqrt{c^*}\right)-\Psi_1^* K_1\left(\rho\beta\sqrt{c^*}\right)\right]}{\Psi_1^* K_1\left(\beta\sqrt{c^*}\right)-\Psi_2^* I_1\left(\beta\sqrt{c^*}\right)+\Psi_3^*} \tag{51}$$

$$\tilde{\sigma}_{rr1}^* = \frac{1}{s}\frac{k^*}{\beta\sqrt{c^*}}\frac{1}{\Psi_1^* K_1\left(\beta\sqrt{c^*}\right)-\Psi_2^* I_1\left(\beta\sqrt{c^*}\right)+\Psi_3^*} \times\left(\frac{2\eta\Psi_1^* F_1^*}{\rho\beta\sqrt{c^*}}+\frac{2\eta\Psi_2^* F_2^*}{\rho\beta\sqrt{c^*}}-\frac{1}{\rho^2}F_3^*\right) \tag{52}$$

$$\tilde{\sigma}_{\theta\theta 1}^* = \frac{1}{s}\frac{k^*}{\beta\sqrt{c^*}}\frac{1}{\Psi_1^* K_1\left(\beta\sqrt{c^*}\right)-\Psi_2^* I_1\left(\beta\sqrt{c^*}\right)+\Psi_3^*}\left(-\frac{2\eta\Psi_1^* F_1^*}{\rho\beta\sqrt{c^*}} -\frac{2\eta\Psi_2^* F_2^*}{\rho\beta\sqrt{c^*}}+\frac{1}{\rho^2}F_3^*-2\eta F_4^*\right) \tag{53}$$

$$\tilde{\sigma}_{zz1}^* = -\frac{1}{s}\frac{k^*}{\beta\sqrt{c^*}}\frac{2\eta F_4^*}{\Psi_1^* K_1\left(\beta\sqrt{c^*}\right)-\Psi_2^* I_1\left(\beta\sqrt{c^*}\right)+\Psi_3^*} \tag{54}$$

$$\tilde{u}_{r1}^* = \frac{1}{s}\frac{k^*}{\beta\sqrt{c^*}}\frac{1}{\Psi_1^* K_1\left(\beta\sqrt{c^*}\right)-\Psi_2^* I_1\left(\beta\sqrt{c^*}\right)+\Psi_3^*} \times\left(-\frac{\eta\Psi_1^* F_1^*}{\beta\sqrt{c^*}}-\frac{\eta\Psi_2^* F_2^*}{\beta\sqrt{c^*}}+\frac{1}{2\rho}F_3^*\right) \tag{55}$$

where:

$$\Psi_1^* = \frac{k^*}{\sqrt{c^*}}I_0\left(\rho_s\beta\sqrt{c^*}\right)K_1(\rho_s\beta)+I_1\left(\rho_s\beta\sqrt{c^*}\right)K_0(\rho_s\beta) \tag{56}$$

$$\Psi_2^* = K_1\left(\rho_s\beta\sqrt{c^*}\right)K_0(\rho_s\beta)-\frac{k^*}{\sqrt{c^*}}K_0\left(\rho_s\beta\sqrt{c^*}\right)K_1(\rho_s\beta) \tag{57}$$

$$\Psi_3^* = \frac{C_W^*\beta k^*}{\sqrt{c^*}}\left[\Psi_2^* I_0\left(\beta\sqrt{c^*}\right)+\Psi_1^* K_0\left(\beta\sqrt{c^*}\right)\right] \tag{58}$$

$$F_1^* = K_1\left(\rho\beta\sqrt{c^*}\right)-K_1\left(\beta\sqrt{c^*}\right)/\rho \tag{59}$$

$$F_2^* = I_1\left(\beta\sqrt{c^*}\right)/\rho-I_1\left(\rho\beta\sqrt{c^*}\right) \tag{60}$$

$$F_3^* = \Psi_2^* I_0\left(\beta\sqrt{c^*}\right)+\Psi_1^* K_0\left(\beta\sqrt{c^*}\right) \tag{61}$$

$$F_4^* = \Psi_2^* I_0\left(\rho\beta\sqrt{c^*}\right)+\Psi_1^* K_0\left(\rho\beta\sqrt{c^*}\right) \tag{62}$$

In the formation zone:

$$\tilde{p}_2^* = \tilde{s}_{h2}^* = \frac{1}{s}\frac{k^*}{\beta\sqrt{c^*}}\frac{K_0(\rho\beta)\left[\Psi_2^* I_0\left(\rho_s\beta\sqrt{c^*}\right)+\Psi_1^* K_0\left(\rho_s\beta\sqrt{c^*}\right)\right]}{K_0(\rho_s\beta)\left[\Psi_1^* K_1\left(\beta\sqrt{c^*}\right)-\Psi_2^* I_1\left(\beta\sqrt{c^*}\right)+\Psi_3^*\right]} \tag{63}$$

$$\tilde{s}_{h2,\rho}^* = -\frac{1}{s}\frac{k^*}{\sqrt{c^*}}\frac{K_1(\rho\beta)\left[\Psi_2^* I_0\left(\rho_s\beta\sqrt{c^*}\right)+\Psi_1^* K_0\left(\rho_s\beta\sqrt{c^*}\right)\right]}{K_0(\rho_s\beta)\left[\Psi_1^* K_1\left(\beta\sqrt{c^*}\right)-\Psi_2^* I_1\left(\beta\sqrt{c^*}\right)+\Psi_3^*\right]} \tag{64}$$

$$\tilde{\sigma}_{rr2}^* = \frac{1}{s}\frac{k^*}{\beta\sqrt{c^*}}\frac{1}{\Psi_1^* K_1\left(\beta\sqrt{c^*}\right)-\Psi_2^* I_1\left(\beta\sqrt{c^*}\right)+\Psi_3^*} \times\left[\frac{2\eta}{\rho\beta}\frac{F_5^* F_8^*}{K_0(\rho_s\beta)}+\frac{2\eta\Psi_2^* F_6^*}{\rho\beta\sqrt{c^*}}+\frac{2\eta\Psi_1^* F_7^*}{\rho\beta\sqrt{c^*}}-\frac{F_3^*}{\rho^2}\right] \tag{65}$$

$$\tilde{\sigma}_{\theta\theta2}^* = \frac{1}{s}\frac{k^*}{\beta\sqrt{c^*}}\frac{1}{\Psi_1^* K_1\left(\beta\sqrt{c^*}\right)-\Psi_2^* I_1\left(\beta\sqrt{c^*}\right)+\Psi_3^*} \times\left[\frac{F_3^*}{\rho^2}-\frac{2\eta}{\rho\beta}\frac{F_8^*\left(F_5^*+\rho\beta K_0(\rho\beta)\right)}{K_0(\rho_s\beta)}-\frac{2\eta\Psi_2^*}{\rho\beta\sqrt{c^*}}F_6^*-\frac{2\eta\Psi_1^*}{\rho\beta\sqrt{c^*}}F_7^*\right] \tag{66}$$

$$\tilde{\sigma}_{zz2}^* = -\frac{1}{s}\frac{k^*}{\beta\sqrt{c^*}}\frac{2\eta K_0(\rho\beta)}{\Psi_1^* K_1\left(\beta\sqrt{c^*}\right)-\Psi_2^* I_1\left(\beta\sqrt{c^*}\right)+\Psi_3^*}\frac{F_8^*}{K_0(\rho_s\beta)} \tag{67}$$

$$\tilde{u}_{r2}^* = \frac{1}{s}\frac{k^*}{\beta\sqrt{c^*}}\frac{1}{\Psi_1^* K_1\left(\beta\sqrt{c^*}\right)-\Psi_2^* I_1\left(\beta\sqrt{c^*}\right)+\Psi_3^*} \times\left[\frac{1}{2\rho}F_3^*-\frac{\eta F_5^* F_8^*}{\beta K_0(\rho_s\beta)}-\frac{\eta\Psi_2^*}{\beta\sqrt{c^*}}F_6^*-\frac{\eta\Psi_1^*}{\beta\sqrt{c^*}}F_7^*\right] \tag{68}$$

where:

$$F_5^* = K_1(\rho\beta)-\rho_s K_1(\rho_s\beta)/\rho \tag{69}$$

$$F_6^* = I_1\left(\beta\sqrt{c^*}\right)/\rho-\rho_s I_1\left(\rho_s\beta\sqrt{c^*}\right)/\rho \tag{70}$$

$$F_7^* = K_1\left(\rho_s\beta\sqrt{c^*}\right)\rho_s/\rho-K_1\left(\beta\sqrt{c^*}\right)/\rho \tag{71}$$

$$F_8^* = \Psi_2^* I_0\left(\rho_s\beta\sqrt{c^*}\right)+\Psi_1^* K_0\left(\rho_s\beta\sqrt{c^*}\right) \tag{72}$$

## 3. Comparison with existing analytical solutions

Verification of the analytical solutions derived above was performed by comparing them to existing solutions in groundwater and poroelastic literature.

### 3.1. Comparison with analytical solutions in groundwater theory

Replacing the specific storage defined in Eq. (10) with the specific storage used in the groundwater flow model Eq. (87) avoids the poroelastic effects, and therefore Eqs. (50) and (63) can be reduced to the solutions of Novakowski (1989).When and the pumping well has a finite diameter but negligibly small storage, setting $C_W^* = 0$ reduces Eqs. (50) and (63) to:

$$\tilde{s}_{h1}^* = \frac{1}{s}\frac{k^*}{\beta\sqrt{c^*}}\frac{\Psi_2^* I_0\left(\rho\beta\sqrt{c^*}\right)+\Psi_1^* K_0\left(\rho\beta\sqrt{c^*}\right)}{\Psi_1^* K_1\left(\beta\sqrt{c^*}\right)-\Psi_2^* I_1\left(\beta\sqrt{c^*}\right)} \tag{73}$$

and:

$$\tilde{s}_{h2}^* = \frac{1}{s}\frac{k^*}{\beta\sqrt{c^*}}\frac{K_0(\rho\beta)\left[\Psi_2^* I_0\left(\rho_s\beta\sqrt{c^*}\right)+\Psi_1^* K_0\left(\rho_s\beta\sqrt{c^*}\right)\right]}{K_0(\rho_s\beta)\left[\Psi_1^* K_1\left(\beta\sqrt{c^*}\right)-\Psi_2^* I_1\left(\beta\sqrt{c^*}\right)\right]} \tag{74}$$

respectively, which agree with the solutions of Yeh et al. (2003). When the fully penetrating pumping well has storage but lacks skin zone, setting $c^* = 1$, $k^* = 1$, and $\rho_s = 1$ reduces Eq. (63) to:

$$\tilde{s}_{h2}^* = \frac{1}{s}\frac{1}{\beta}\frac{K_0(\rho\beta)}{\left[K_1(\beta)+\beta C_W^* K_0(\beta)\right]} \tag{75}$$

which is identical to Eq. (2) of Papadopulos and Cooper (1967). When the pumping well has an infinitesimal radius and a finite-thickness skin zone, setting $\beta \to 0$ and using $\lim_{x\to 0}[xK_1(x)] = 1$ reduces Eqs. (50) and (63) to:

$$\tilde{s}_{h1}^* = \frac{k^*}{s}\left[K_0\left(\rho\beta\sqrt{c^*}\right)+\frac{\Psi_2^*}{\Psi_1^*}I_0\left(\rho\beta\sqrt{c^*}\right)\right] \tag{76}$$

and:

$$\tilde{s}_{h2}^* = \frac{1}{s}\frac{k^*}{\rho_s\beta\sqrt{c^*}}\frac{K_0(\rho\beta)}{\Psi_1^*} \tag{77}$$

respectively, which are consistent with Eqs. (16) and (17) of Butler (1988).

When the skin zone is absent, the two equations further reduce to:

$$\tilde{s}_{h2}^* = \frac{K_0(\rho\beta)}{s} \tag{78}$$

which is the Laplace transform of the Theis solution (Theis, 1935).

### 3.2. Comparison with analytical solutions in poroelastic theory

When the pumping well has a finite radius and no skin zone but negligibly small storage in a uniform aquifer, setting $C_W^* = 0$, $c^* = 1$, $k^* = 1$, and $\rho_s = 1$, reduces Eq. (63) to:

$$\tilde{s}_{h2}^* = \frac{1}{s}\frac{1}{\beta}\frac{K_0(\rho\beta)}{K_1(\beta)} \tag{79}$$

which is in agreement with Eq. (7.645) of Cheng (2016). Eqs. (52) and (65) reduce to:

$$\tilde{\sigma}_{rr1}^* = \tilde{\sigma}_{rr2}^* = \frac{1}{s}\frac{2\eta}{\rho\beta^2}\left[\frac{K_1(\rho\beta)}{K_1(\beta)}-\frac{1}{\rho}\right]-\frac{1}{s}\frac{1}{\rho^2\beta}\frac{K_0(\beta)}{K_1(\beta)} \tag{80}$$

Eqs. (53) and (66) reduce to:

$$\tilde{\sigma}_{\theta\theta1}^* = \tilde{\sigma}_{\theta\theta2}^* = \frac{1}{s}\frac{1}{\rho^2\beta}\frac{K_0(\beta)}{K_1(\beta)}-\frac{2\eta}{s}\left[\frac{K_1(\rho\beta)}{\rho\beta^2 K_1(\beta)}-\frac{1}{\rho^2\beta^2}+\frac{K_0(\rho\beta)}{\beta K_1(\beta)}\right] \tag{81}$$

From Eqs. (79) to (81), we can get the Terzaghi's effective radial and hoop stresses as follows:

$$\tilde{\sigma}_{rr}^{*\prime} = \frac{1}{s}\frac{2\eta}{\rho\beta^2}\left[\frac{K_1(\rho\beta)}{K_1(\beta)}-\frac{1}{\rho}\right]-\frac{1}{s}\frac{1}{\rho^2\beta}\frac{K_0(\beta)}{K_1(\beta)}+\frac{1}{s}\frac{1}{\beta}\frac{K_0(\rho\beta)}{K_1(\beta)} \tag{82}$$

$$\tilde{\sigma}_{\theta\theta}^{*\prime} = \frac{1}{s}\frac{1}{\rho^2\beta}\frac{K_0(\beta)}{K_1(\beta)}-\frac{2\eta}{s}\left[\frac{K_1(\rho\beta)}{\rho\beta^2 K_1(\beta)}-\frac{1}{\rho^2\beta^2}+\frac{K_0(\rho\beta)}{\beta K_1(\beta)}\right]+\frac{1}{s}\frac{1}{\beta}\frac{K_0(\rho\beta)}{K_1(\beta)} \tag{83}$$

Eqs. (82) and (83) agree with Eqs. (7.734) and (7.735) of Cheng (2016), respectively.

## 4. Results and discussion

To obtain the solutions in the time domain, we carried out an inverse Laplace transform using the Stehfest algorithm (Stehfest, 1970) because of its computational efficiency and accuracy, which is given by:

$$f(t) = \frac{\ln 2}{t}\sum_{i=1}^{N} V_i\tilde{f}\left(\frac{\ln 2}{t}i\right) \tag{84}$$

where:

$$V_i = (-1)^{i+N/2}\sum_{k=\left\lfloor\frac{i+1}{2}\right\rfloor}^{\min(i,N/2)}\frac{k^{N/2}(2k)!}{(N/2-k)!k!(k-1)!(i-k)!(2k-i)!} \tag{85}$$

**Table 1**
Hydromechanical properties used in the numerical analysis.

| Symbol | Definition | Berea sandstone | Tennessee marble |
|---|---|---|---|
| $G$ | Shear modulus | 6 GPa | 24 GPa |
| $K$ | Bulk modulus | 8 GPa | 40 GPa |
| $K_s$ | Grain bulk modulus | 36 GPa | 50 GPa |
| $K_f$ | Fluid bulk modulus | 2.25 GPa | 2.25 GPa |
| $\phi$ | Porosity | 0.19 | 0.02 |
| $k$ | Intrinsic permeability | $1.9 \times 10^{-13}$ m$^2$ | $1.0 \times 10^{-19}$ m$^2$ |
| $\mu$ | Fluid viscosity | $1.0 \times 10^{-3}$ Pa-s | $1.0 \times 10^{-3}$ Pa-s |
| $\alpha$ | Biot coefficient | 0.778 | 0.2 |
| $B$ | Skempton coefficient | 0.551 | 0.371 |

We use $N$= 10 in our numerical inversion. The main challenges in the numerical inversion of the Laplace transform lie in the singularity of the modified Bessel function of first kind of zero order and first order at a very large $s$. The following asymptotic expansions are used for a large $s$ (Abramowitz and Stegun, 1964)

$$I_0(s) \approx \frac{\exp(s)}{\sqrt{2\pi s}}\left(1+\frac{1}{8s}+\frac{9}{128s^2}\right), \qquad I_1(s) \approx \frac{\exp(s)}{\sqrt{2\pi s}}\left(1-\frac{3}{8s}-\frac{15}{128s^2}\right) \tag{86}$$

In the numerical examples considered here, sandstone and marble are used as two representative materials for illustrative purposes. These two rocks represent systems with widely different hydromechanical properties. Sandstone aquifers are prominently featured in groundwater resources studies, whereas the study of marble reservoirs is more useful for applications in which low permeability is encountered or is desired, such as studying enhanced geothermal systems, nuclear waste repositories, or carbon sequestration methods. Table 1 lists the hydromechanical properties of Berea sandstone and Tennessee marble as reported in Wang (2000) and Cheng (2016). We focused on the effects of poroelastic coupling on the transient drawdown behavior. A parametric study was performed to investigate the sensitivity of drawdown to variations in physical parameters, including skin type, skin thickness, and wellbore storage.

### 4.1. Effects of poroelasticity

Before we explore the effects of poroelastic deformation on the transient drawdown, it is instructive to compare the fully coupled poroelastic formulations to the uncoupled groundwater flow theory. The governing equation for transient flow widely used in conventional groundwater theory is (Yeh and Chang, 2013):

$$\nabla^2 s_h = \frac{S_s}{K}\frac{\partial s_h}{\partial t} \tag{87}$$

where $s_h$ is the drawdown in the aquifer, $S_s$ is the specific storage coefficient, and $K$ is the hydraulic conductivity. Hydraulic conductivity, $K$, is related to permeability, $k$, by$K = \rho_f g k/\mu$. Under the assumption of constant vertical stress and uniaxial deformation, the specific storage in classical groundwater theory is given as (Jacob, 1940):

$$S_s = \rho g\left(\frac{1}{K_V}+\frac{\phi}{K_f}\right) \tag{88}$$

In the Jacob's equation for specific storage that is commonly used in groundwater flow theory, solid grains are assumed incompressible, which results in a higher specific storage than the storage calculated using Eq. (10) in poroelasticity. Therefore, the uncoupled groundwater theory overestimates the specific storage, and consequently underestimates the hydraulic diffusivity and predicts a lower drawdown compared with the coupled poroelasticity under identical pumping test conditions. The second key difference between groundwater theory and poroelasticity can be observed by comparing Eqs. (9) and (87). In poroelasticity, the linear combination of pore pressure and mean stress follows the diffusion equation. Mathematically, the rate of changes in mean stress with respect to time is equivalent to a fluid source. In groundwater theory, however, hydraulic drawdown (and therefore pore pressure change) satisfies a homogeneous diffusion equation.

To separate the effect of poroelastic deformation from wellbore storage and skin zone, we use the following parameters: $C_W^* = 0$, $c^* = 1$, and $k^* = 1$. Figs. 2a and b show a comparison of the dimensionless drawdown predicted using groundwater theory and coupled poroelasticity as a function of radial distance from the pumping well at various nondimensional times for sandstone and marble, respectively. At a given time, hydraulic drawdown decreases monotonically with increasing distance from the pumping well. At the pumping well, drawdown increases steadily with increasing time. The general trends of the radial distribution of drawdown are similar for sandstone and marble, and groundwater theory is seen to underestimate the drawdown at the pumping well. For sandstone, the drawdown distribution obtained from poroelasticity is slightly higher than that obtained from groundwater theory at the same time. For marble, the observed difference in drawdown distribution is significantly higher. This phenomenon can be explained by examining the difference in specific storage in Eqs. (10) and (88) and noting the contribution of volumetric deformation to the changes in pore pressure. For marble, the calculated specific storage using Jacob's Eq. (88) is 75% larger than the specific storage calculated using Eq. (10), which incorporated poroelasticity. For sandstone, the difference is approximately 8%. Therefore, for marble, groundwater theory overestimates specific storage and significantly underestimates the hydraulic diffusivity, leading to a smaller magnitude and slower evolution of drawdown. Furthermore, Eq. (5) indicates that pore pressure changes (drawdowns) come from two sources: (1) fluid released from storage and (2) volumetric deformation of the matrix due to the Skempton effect. The groundwater theory underestimates the drawdown without capturing pumping-induced volumetric deformation. The sharp difference in drawdown prediction for marble highlights the significance of including poroelasticity in estimating hydraulic parameters based on pumping test conducted in low-permeable aquifers and reservoirs.

Using the same parameters as those used in Figs. 2, 3a and 3b show the influence of poroelasticity on the radial distribution of the nondimensional drawdown gradient at different normalized times for sandstone and marble, respectively. The nondimensional drawdown analysis provides a general hydrodynamic conceptual framework to represent the transient evolution of the shape of the pressure-front pulse that diffuses throughout an aquifer during pumping (Barker, 1988; Ferroud et al., 2019). It is evident that at a given location, the drawdown gradient deceases with increasing time. At a given time, drawdown gradient decreases steadily with increases in the radial distance from the pumping well. As expected, the drawdown gradient for sandstone is marginally sensitive to poroelastic deformation. For marble, groundwater theory underestimates the drawdown gradient slightly at the beginning of the pumping test and the differences increases with increasing time.

### 4.2. Effects of skin types

To examine the effects of skin types on aquifer response, temporal evolution of dimensionless drawdown distributions are shown in Figs. 4 and 5 at the pumping well ($\rho = 1$) and at a hypothetical observation well located at $\rho = 100$ for conditions described by $\rho_s$ =3, $C_W^* = 0$, with $k^*$ ranging from 0.1 to 10. Note that $k^*$=1 represents the case of a homogeneous formation, whereas $k^*$=0.1 and $k^*$=10 represent the negative and positive skin zone, respectively. The pumping well with a positive skin zone has a remarkably larger drawdown than those without a skin zone or with a negative skin zone. This can be explained by observing that in the case of a positive skin, the permeability of the skin zone is smaller than the permeability of the formation. It also takes longer to compensate for the diffusion induced pressure loss to maintain a constant pumping rate at the wellbore. For a negative skin, pore pressure diffuses quickly from the formation to the wellbore, and so a small draw-

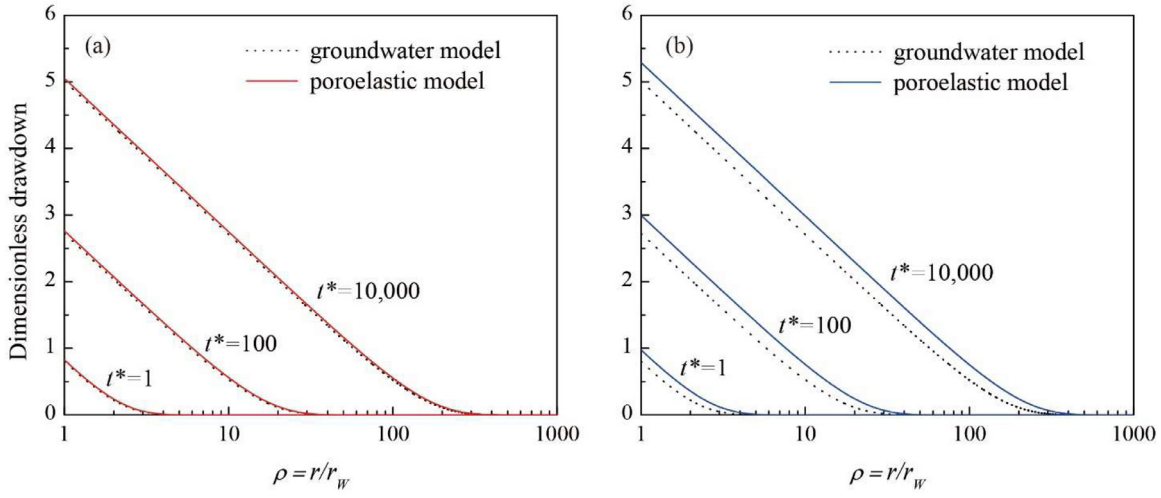


**Fig. 2.** Poroelastic effects on the radial distribution of dimensionless drawdown in (a) sandstone and (b) marble at various dimensionless times for $C_W^* = 0$, $c^* = 1$, and $k^* = 1$.

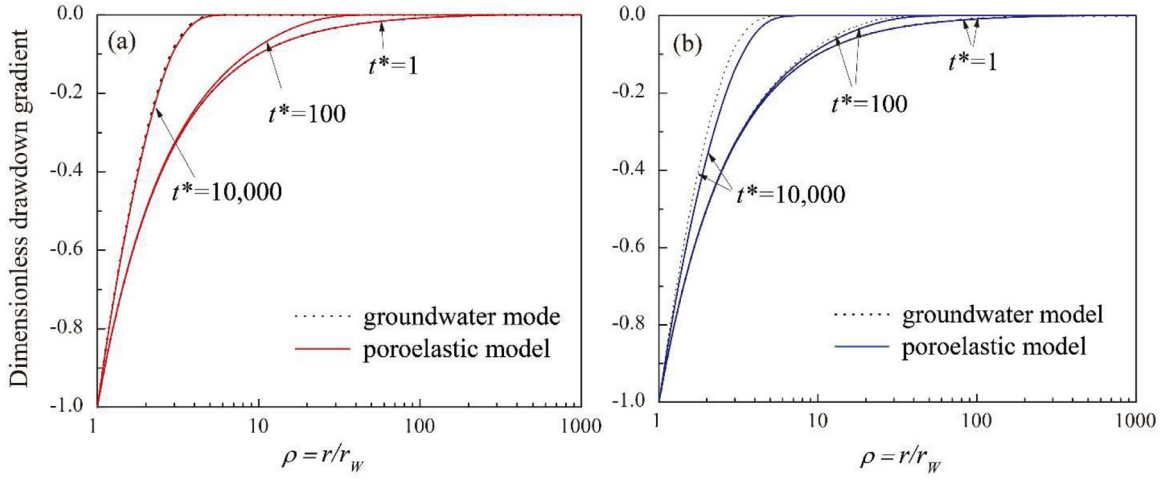


**Fig. 3.** Poroelastic effects on the radial distribution of dimensionless drawdown gradient in (a) sandstone and (b) marble at various dimensionless times for $C_W^* = 0$, $c^* = 1$, and $k^* = 1$.

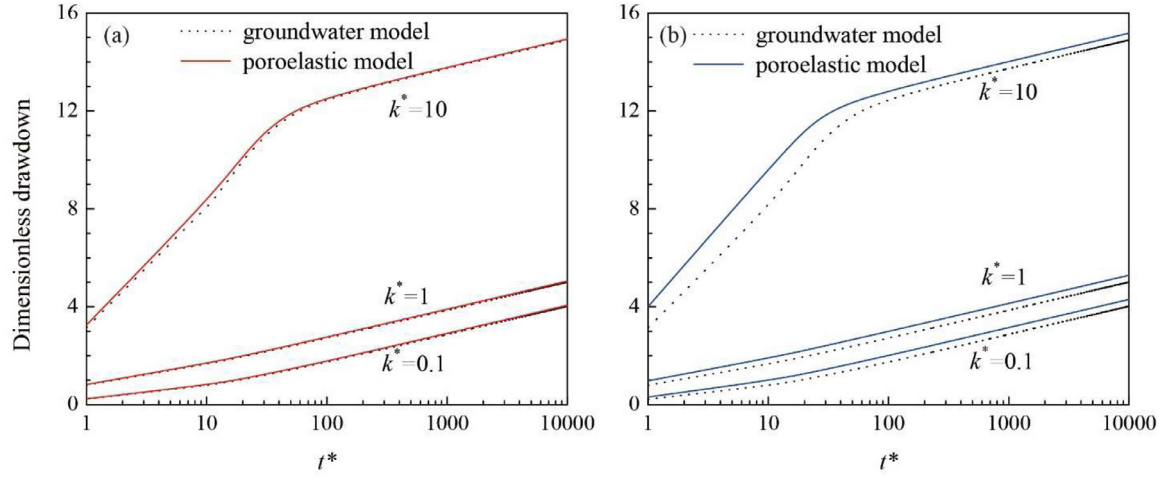


**Fig. 4.** Effects of skin types on temporal evolution of dimensionless drawdown in (a) sandstone and (b) marble at the pumping well ($\rho = 1$) for $\rho_s$ =3, and $C_W^* = 0$.

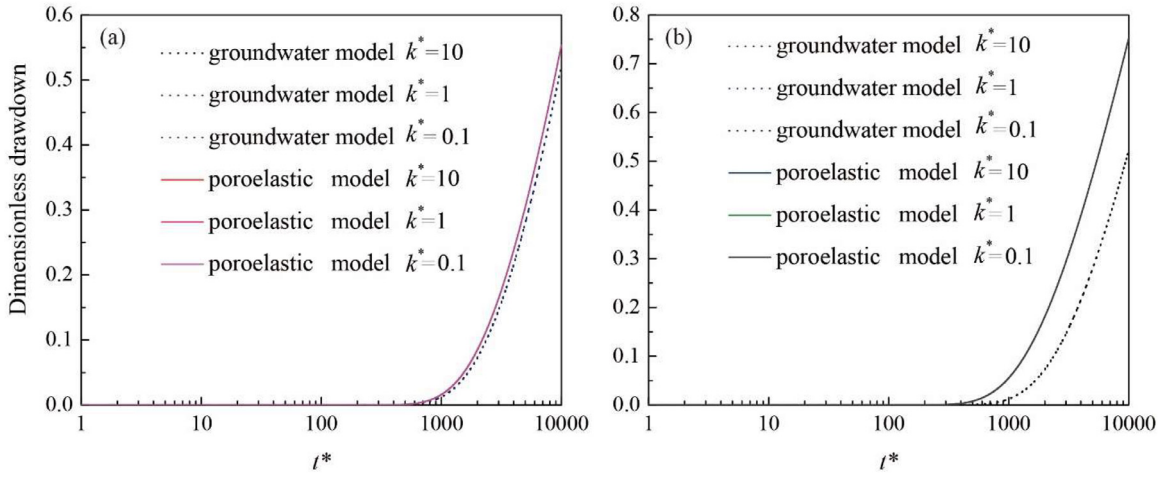


**Fig. 5.** Effects of skin types on temporal evolution of dimensionless drawdown in (a) sandstone and (b) marble at the observation well ($\rho$ = 100) for $\rho_s$ =3, and $C_W^* = 0$.

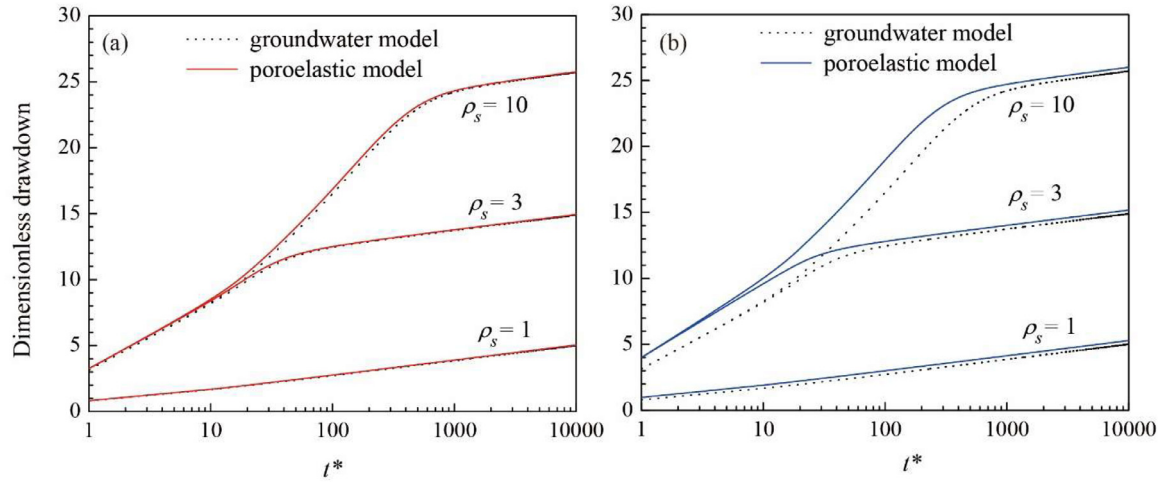


**Fig. 6.** Effects of skin thickness on temporal evolution of dimensionless drawdown in (a) sandstone and (b) marble at the pumping well ($\rho$ = 1) for k*=10, and $C_W^* = 0$.

down (pore pressure decrease) is observed at the pumping well. Drawdown is more affected by the positive skin than by the negative skin, especially in the vicinity of the pumping well. At the observation well ($\rho = 100$), the skin effect is negligible as seen by a nearly complete overlap of drawdown curves for the three $k^*$ values in Fig. 5. For sandstone, the magnitude of drawdown at the wellbore predicted from groundwater theory is close to that predicted from poroelasticity. For marble, the magnitude of drawdown at the pumping well obtained from groundwater theory is smaller than that obtained from poroelasticity, and the difference is more pronounced at early pumping time ($t^*$<30). At the observation well, the magnitude of poroelasticity-based drawdown is significantly greater than that predicted from groundwater theory at a long pumping time ($t^*$>1000). For example, at $t^*$=10,000 the drawdown at $\rho$ = 100 from poroelasticity is approximately 36% greater than that predicted from groundwater theory.

### 4.3. Effects of skin thickness

To investigate the sensitivity of drawdown to a pumping test in a well with variable skin thickness, we studied a well with positive skin ($k^*$=10) of variable thickness ($\rho_s$ =1, 3, and 10) and plotted the evolution of drawdown at the pumping well ($\rho$ = 1) and at the observation well ($\rho = 100$) in Figs. 6 and 7, respectively. Note that $\rho_s$ =1 denotes the case of a pumping well without a skin zone. It is evident from Fig. 6 that the drawdown at the pumping well increases with the increasing thickness of the positive skin zone. A positive skin means a lower permeability in the skin zone than in the formation, and therefore a thicker positive skin means that groundwater replenishment into the well takes longer through the skin zone. At the observation well ($\rho = 100$), the drawdowns are not sensitive to the thickness of the skin zone, which suggests that skin zone properties (type and thickness) play a minor role in far-field drawdowns.

### 4.4. Effects of wellbore storage

To investigate the effects of wellbore storage on aquifer performance in response to pumping tests from wells with different storage, we measured the drawdowns at the pumping well ($\rho$ = 1) and at the observation well ($\rho$ = 100). Figs. 8 and 9 show the pumping and observation well drawdowns corresponding wellbore storage based on the following physical parameters: $\rho_s$ =3, $k^*$=10, and $c^*$=10. There are two noteworthy features. First, wellbore storage delays the migration of groundwater from the formation to the well. Increasing wellbore storage results in an appreciable decrease in drawdown at the pumping well and at the observation well (which can be seen by comparing the extent of the vertical axes in Figs. 8 and 9 to those of Fig. 4 through 7). Second,

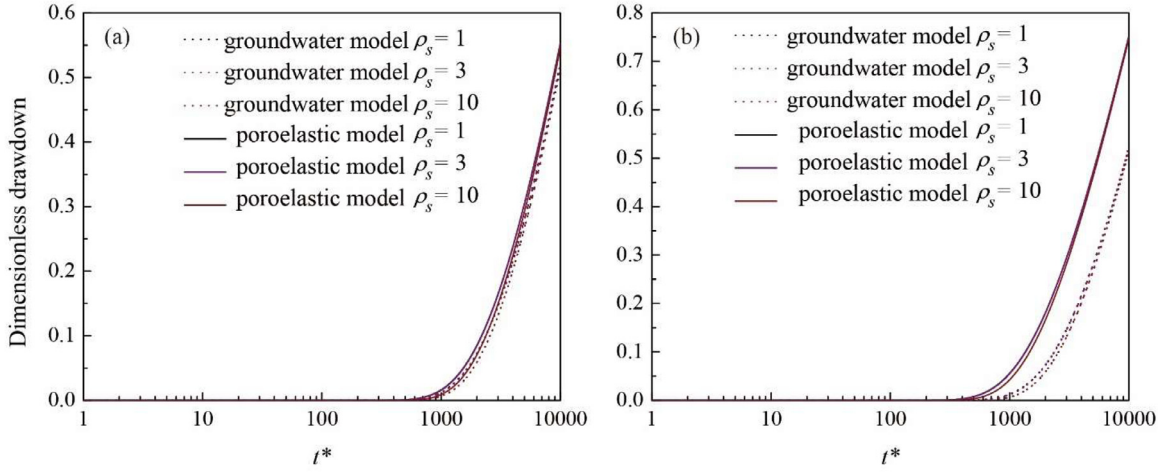


**Fig. 7.** Effects of skin thickness on temporal evolution of dimensionless drawdown in (a) sandstone and (b) marble at the observation well ($\rho$ = 100) for $k^*$=10, and $C_W^*$ = 0.

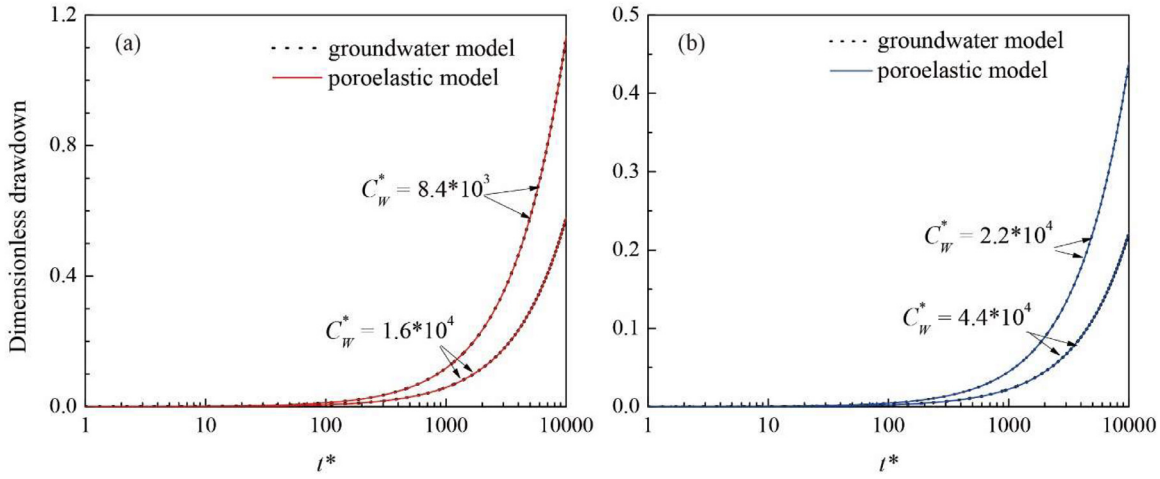


**Fig. 8.** Effects of wellbore storage on the temporal evolution of dimensionless drawdown in (a) sandstone and (b) marble at the pumping well ($\rho$ = 1) for $\rho_s$ =3, $k^*$=10, and $c^*$=10.

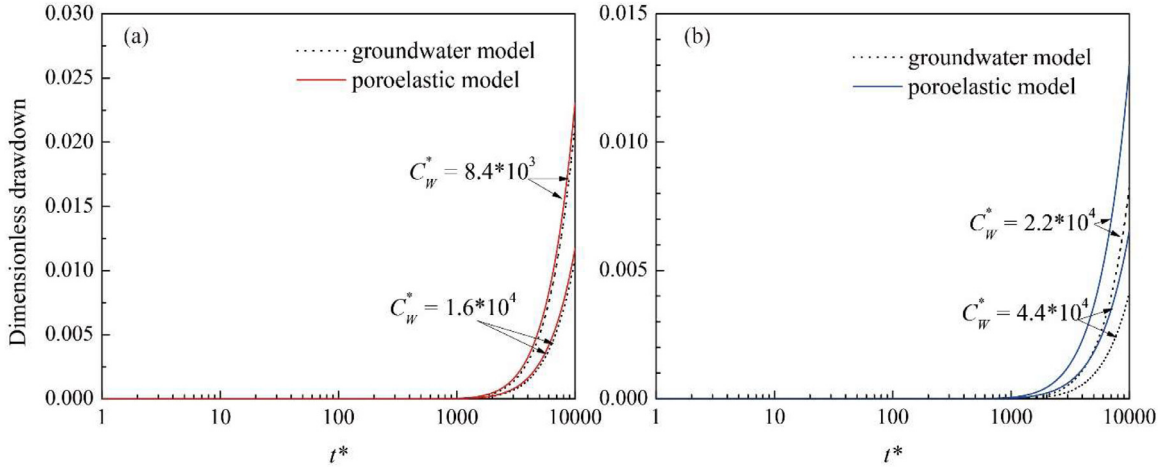


**Fig. 9.** Effects of wellbore storage on temporal evolution of dimensionless drawdown in (a) sandstone and (b) marble at the observation well ($\rho$ = 100) for $\rho_s$ =3, $k^*$=10, and $c^*$=10.

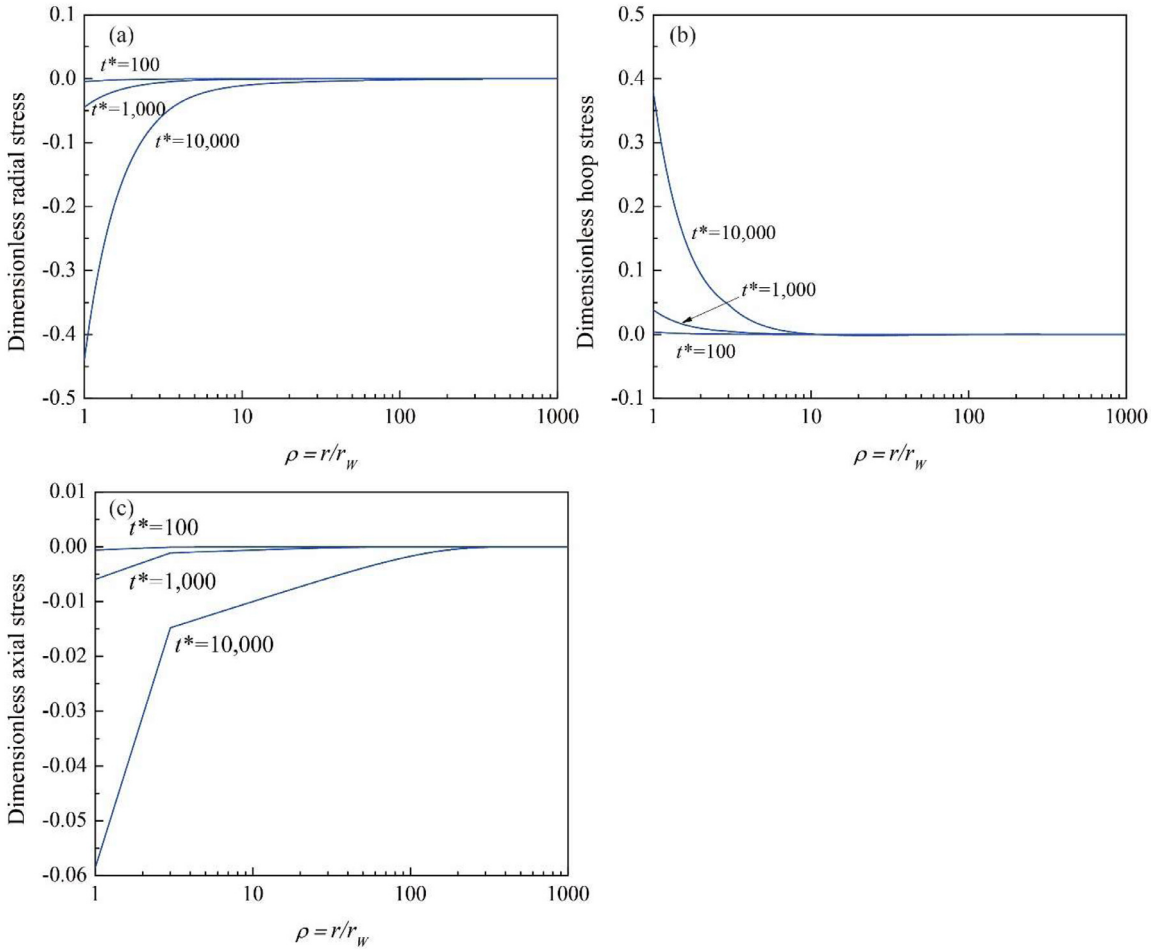


**Fig. 10.** Pumping induced dimensionless (a) radial, (b) hoop, and (c) axial stress changes in marble for $\rho_s$ =3, $k^*$=10, and $C_W^* = 2.2 * 10^4$.

poroelastic effect is largely masked by the wellbore storage effect, so the drawdown predicted at the pumping well using groundwater theory is indistinguishable from drawdown associated with poroelasticity. This condition is applicable to both sandstone and marble, and it is more pronounced in the vicinity of the pumping well.

### 4.5. Pumping induced stress changes

For illustrative purposes, Fig. 10 shows the pumping induced radial, hoop, and axial stresses as functions of radial distance at various dimensionless times for marble with the following physical parameters: $\rho_s$ =3, $k^*$=10, and $C_W^* = 2.2 * 10^4$. It is evident that poroelastic stresses develop significantly in the skin zone, especially at early time. At a given time, induced stresses drop sharply with increasing distance from the pumping well. At a given location, compressive hoop stress and tensile radial/axial stress progressively increase with time. The axial stress exhibits a sharp change in slope at the interface of the skin zone with the formation (set at $\rho$ =3 in these examples). The magnitude of axial stress is comparatively smaller than the magnitude of radial and hoop stresses, but the axial stress decreases more slowly with respect to distance, resulting in appreciable values of axial stress far away from the pumping well at late times. The hoop stress is directly related to the borehole integrity (i.e., when the Terzaghi effective hoop stress at the borehole wall reaches the tensile strength of the rock matrix, tensile fracture initiates at the borehole wall and breakdown occurs). Eq. (53) and Fig. (10b) can therefore be used to set the upper-bound limits for pumping rates, which would generate measurable pressure drawdowns without causing wellbore breakdown.

## 5. Conclusions

This paper derives analytical solutions for transient flow to a finite-radius well in a poroelastic confined aquifer that is subjected to a constant-rate pumping. The solutions presented herein, which unify the groundwater solutions of Novakowski (1989) and the poroelasticity solutions of Cheng (2016) simultaneously account for the effects and interactions of a finite-thickness skin zone, wellbore storage, and poroelastic deformation on hydraulic drawdown in the pumping well and in the observation wells. For a uniform aquifer and a finite radius well without storage, the presented Laplace domain solutions have been shown to reduce to the Cheng (2016) solution. When the combined effects of wellbore storage and finite-thickness skin zone are significant but poroelastic effect is not strong, our solutions agree with those presented in Novakowski (1989). Therefore, the following conclusions can be drawn from this study:

(1) For constant-rate pumping tests conducted in low-permeable, confined hard rocks, groundwater theory significantly underestimates the hydraulic drawdown in the pumping well compared with the drawdown predicted from poroelasticity, especially when a positive skin is present. Hydraulic drawdowns in far-field observation wells are sensitive to poroelastic effects. For high-permeable rocks, there is a slight difference between the drawdowns predicted from classic groundwater theory and poroelasticity.
(2) Under otherwise same conditions, a wellbore with a positive skin undergoes greater drawdowns than wellbores with a negative skin or without any skin. The well skin zone has a negligibly small effect on far-field drawdowns.

(3) Wellbore storage significantly delays drawdowns at the pumping well and tends to mask the poroelastic effect in the vicinity of the pumping well.

The solutions developed in this paper can be used to investigate the effects of poroelastic deformation, skin zone properties, and wellbore storage on the drawdown distribution in the pumping well, as well as in the observation wells. This information provides useful guidance to practitioners to analyze and interpret pumping tests, determine the optimal placement of observation wells, and set appropriate well operation parameters to ensure wellbore integrity.

## Declaration of Competing Interest

The authors declare that they have no conflict of interest.

## CRediT authorship contribution statement

**Zhiqiang Fan:** Conceptualization, Methodology, Validation, Formal analysis, Writing - original draft, Writing - review & editing. **Rishi Parashar:** Writing - review & editing.

## Acknowledgments

We thank the Associate Editor, Nicole Daman, and five anonymous reviewers for their helpful comments that greatly improved the paper. The first author would like to acknowledge the support from Nell J. Redfield foundation, the Maki Endowment, and the Desert Research Institute.

## Appendix A. Derivation of Eqs. (26–46)

Applying the Laplace transform of governing Eq. (8) for fluid variation, $\zeta$, in the skin zone with respect to time, $t$, yields:

$$\frac{d^2\tilde{\zeta}_1}{dr^2}+\frac{1}{r}\frac{d\tilde{\zeta}_1}{dr}-\frac{s}{c_1}\tilde{\zeta}_1=0 \tag{A.1}$$

The general solution of (A.1) is:

$$\tilde{\zeta}_1(r,s)=A_1(r,s)I_0(r\sqrt{s/c_1})+A_2(r,s)K_0(r\sqrt{s/c_1}) \tag{A.2}$$

where $A_1$ and $A_2$ are two integration constants.

Applying the Laplace transform to Eq. (13) and integrating the result in:

$$\tilde{\varepsilon}_{kk1}(r,s)=\frac{\eta}{GS_1}\tilde{\zeta}_1(r,s)+2A_3 \tag{A.3}$$

where $\eta=\alpha\frac{1-2\nu}{2(1-\nu)}$ and $S_1=\frac{(1-\nu_u)(1-2\nu)}{M(1-\nu)(1-2\nu_u)}$ are two poroelastic constants, and $A_3$ is an integration constant.

Substituting and integrating Eq. (7) into the above equation gives:

$$\begin{aligned}\tilde{u}_{r1}=&\frac{1}{r}\frac{\eta}{GS_1}\int r\tilde{\zeta}_1dr+A_3r+\frac{A_4}{r}=\frac{\eta}{GS_1}A_1\frac{I_1(r\sqrt{s/c_1})}{\sqrt{s/c_1}}\\&-\frac{\eta}{GS_1}A_2\frac{K_1(r\sqrt{s/c_1})}{\sqrt{s/c_1}}+A_3r+\frac{A_4}{r}\end{aligned} \tag{A.4}$$

where $A_4$ is an integration constant.

Using Eq. (6), we can get the Laplace transform of strain components. Then, the skin zone stress components, pore pressure, and fluid flux in the Laplace domain are given by:

$$\tilde{\sigma}_{rr1}=-\frac{2\eta}{S_1}A_1\frac{I_1(r\sqrt{s/c_1})}{r\sqrt{s/c_1}}+\frac{2\eta}{S_1}A_2\frac{K_1(r\sqrt{s/c_1})}{r\sqrt{s/c_1}}+\frac{2G}{1-2\nu_u}A_3-\frac{2G}{r^2}A_4 \tag{A.5}$$

$$\begin{aligned}\tilde{\sigma}_{\theta\theta1}=&\frac{2\eta}{S_1}A_1\left[\frac{I_1\left(r\sqrt{s/c_1}\right)}{r\sqrt{s/c_1}}-I_0\left(r\sqrt{s/c_1}\right)\right]-\frac{2\eta}{S_1}A_2\\&\times\left[\frac{K_1\left(r\sqrt{s/c_1}\right)}{r\sqrt{s/c_1}}+K_0\left(r\sqrt{s/c_1}\right)\right]+\frac{2G}{1-2\nu_u}A_3+\frac{2G}{r^2}A_4\end{aligned} \tag{A.6}$$

$$\tilde{\sigma}_{zz1}=-\frac{2\eta}{S_1}A_1I_0(r\sqrt{s/c_1})-\frac{2\eta}{S_1}A_2K_0(r\sqrt{s/c_1})+\frac{4G\nu_u}{1-2\nu_u}A_3 \tag{A.7}$$

$$\tilde{p}_1=A_1I_0(r\sqrt{s/c_1})/S_1+A_2K_0(r\sqrt{s/c_1})/S_1-2\alpha MA_3 \tag{A.8}$$

$$\tilde{q}_{r1}=-A_1\frac{k_1}{\mu}\sqrt{s/c_1}I_1\left(r\sqrt{s/c_1}\right)/S_1+A_2\frac{k_1}{\mu}\sqrt{s/c_1}K_1\left(r\sqrt{s/c_1}\right)/S_1 \tag{A.9}$$

Similarly, we get the Laplace transform of stress, pore pressure, displacement, and variation of fluid in the formation as follows:

$$\tilde{\zeta}_2(r,s)=B_1(r,s)I_0(r\sqrt{s/c_2})+B_2(r,s)K_0(r\sqrt{s/c_2}) \tag{A.10}$$

$$\tilde{\sigma}_{rr2}=-\frac{2\eta}{S_2}B_1\frac{I_1(r\sqrt{s/c_2})}{r\sqrt{s/c_2}}+\frac{2\eta}{S_2}B_2\frac{K_1(r\sqrt{s/c_2})}{r\sqrt{s/c_2}}+\frac{2G}{1-2\nu_u}B_3-\frac{2G}{r^2}B_4 \tag{A.11}$$

$$\begin{aligned}\tilde{\sigma}_{\theta\theta2}=&\frac{2\eta}{S_2}B_1\left[\frac{I_1\left(r\sqrt{s/c_2}\right)}{r\sqrt{s/c_2}}-I_0\left(r\sqrt{s/c_2}\right)\right]-\frac{2\eta}{S_2}B_2\\&\times\left[\frac{K_1\left(r\sqrt{s/c_2}\right)}{r\sqrt{s/c_2}}+K_0\left(r\sqrt{s/c_2}\right)\right]+\frac{2G}{1-2\nu_u}B_3+\frac{2G}{r^2}B_4\end{aligned} \tag{A.12}$$

$$\tilde{\sigma}_{zz2}=-\frac{2\eta}{S_2}B_1I_0\left(r\sqrt{s/c_2}\right)-\frac{2\eta}{S_2}B_2K_0\left(r\sqrt{s/c_2}\right)+\frac{4G\nu_u}{1-2\nu_u}B_3 \tag{A.13}$$

$$\tilde{p}_2=\frac{1}{S_2}B_1I_0(r\sqrt{s/c_2})+\frac{1}{S_2}B_2K_0(r\sqrt{s/c_2})-2\alpha MB_3 \tag{A.14}$$

$$\tilde{q}_{r2}=-B_1\frac{k_2}{\mu}\sqrt{s/c_2}I_1\left(r\sqrt{s/c_2}\right)/S_2+B_2\frac{k_2}{\mu}\sqrt{s/c_2}K_1\left(r\sqrt{s/c_2}\right)/S_2 \tag{A.15}$$

where $B_1$-$B_4$ are constants to de determined by the boundary conditions and continuity conditions at the skin/formation interface.

The boundary condition (19) requires that:

$$B_1=B_3=0 \tag{A.16}$$

Application of the Laplace transform to the boundary conditions at the wellbore (20)-(21) using equations (A.5) and (A.8) yields:

$$\begin{aligned}&-\frac{2\eta}{S_1}A_1\frac{I_1(r_W\sqrt{s/c_1})}{r_W\sqrt{s/c_1}}+\frac{2\eta}{S_1}A_2\frac{K_1(r_W\sqrt{s/c_1})}{r_W\sqrt{s/c_1}}+\frac{2G}{1-2\nu_u}A_3-\frac{2G}{r_W^2}A_4=\\&-\left[A_1I_0(r_W\sqrt{s/c_1})/S_1+A_2K_0(r_W\sqrt{s/c_1})/S_1-2\alpha MA_3\right]\end{aligned} \tag{A.17}$$

$$\begin{aligned}&2\pi r_Wb\frac{k_1}{\mu}\left[\frac{A_1}{S_1}\sqrt{\frac{s}{c_1}}I_1(r_W\sqrt{s/c_1})-\frac{A_2}{S_1}\sqrt{\frac{s}{c_1}}K_1(r_W\sqrt{s/c_1})\right]=\\&\frac{C_Ws}{\rho_fg}\left[\frac{A_1}{S_1}I_0(r_W\sqrt{s/c_1})+\frac{A_2}{S_1}K_0(r_W\sqrt{s/c_1})-2\alpha MA_3\right]-\frac{Q}{s}\end{aligned} \tag{A.18}$$

At the interface between the skin zone and formation zone, the continuity of radial displacement, radial stress, pore pressure, and fluid flux

requires that:

$$\frac{\eta}{GS_1}A_1\frac{I_1(r_S\sqrt{s/c_1})}{\sqrt{s/c_1}}-\frac{\eta}{GS_1}A_2\frac{K_1(r_S\sqrt{s/c_1})}{\sqrt{s/c_1}}+A_3r_S+\frac{A_4}{r_S}$$
$$=-\frac{\eta}{GS_2}B_2\frac{K_1(r_S\sqrt{s/c_2})}{\sqrt{s/c_2}}+\frac{B_4}{r_S} \quad (A.19)$$

$$-\frac{2\eta}{S_1}A_1\frac{I_1(r_S\sqrt{s/c_1})}{r_S\sqrt{s/c_1}}+\frac{2\eta}{S_1}A_2\frac{K_1(r_S\sqrt{s/c_1})}{r_S\sqrt{s/c_1}}+\frac{2G}{1-2\nu_u}A_3$$
$$-\frac{2G}{r_S^2}A_4=\frac{2\eta}{S_2}B_2\frac{K_1(r_S\sqrt{s/c_2})}{r_S\sqrt{s/c_2}}-\frac{2G}{r_S^2}B_4 \quad (A.20)$$

$$A_1I_0(r_S\sqrt{s/c_1})/S_1+A_2K_0(r_S\sqrt{s/c_1})/S_1-2\alpha MA_3=B_2K_0(r_S\sqrt{s/c_2})/S_2 \quad (A.21)$$

$$-A_1\frac{k_1}{\mu}\sqrt{s/c_1}I_1\left(r_S\sqrt{s/c_1}\right)/S_1+A_2\frac{k_1}{\mu}\sqrt{s/c_1}K_1\left(r_S\sqrt{s/c_1}\right)/S_1$$
$$=B_2\frac{k_2}{\mu}K_1\left(r_S\sqrt{s/c_2}\right)/S_2 \quad (A.22)$$

Eqs. (A.17) to (A.22) are solved simultaneously to determine the remaining constants $A_1$ to $A_4$, $B_2$ and $B_4$, which are then substituted back into Eqs. (A.5) to (A.15) to get the Laplace domain solutions for stress, pore pressure, and displacement in the skin zone and formation zone.

## References


Abousleiman, Y., Chen, S., 2010. Poromechanics response of an inclined borehole subject to in-situ stress and finite length fluid discharge. J. Mech. Mater. Struct. 5, 47–66. https://doi.org/10.2140/jomms.2010.5.47.

Abramowitz, M., Stegun, I.A., 1964. Handbook of Mathematical Functions. Dover Publications, New York.

Barker, J.A., 1988. A generalized radial flow model for hydraulic tests in fractured rock. Water Resour. Res. 24 (10), 1796–1804.

Belmokhtar, M., Delage, P., Ghabezloo, S., Tang, A.-M., Menaceur, H., Conil, N., 2016. Poroelasticity of the Callovo–Oxfordian claystone. Rock Mech. Rock Eng. 50, 871–889. https://doi.org/10.1007/s00603-016-1137-3.

Berg, S.J., Hsieh, P.A., Illman, W.A., 2011. Estimating hydraulic parameters when poroelastic effects are significant. Groundwater 49, 815–829. https://doi.org/10.1111/j.1745-6584.2010.00781.x.

Burbey, T., 1999. Effects of horizontal strain in estimating specific storage and compaction in confined and leaky aquifer systems. Hydrogeol. J. 7, 521–532. https://doi.org/10.1007/s100400050225.

Burbey, T., 2003. Use of time–subsidence data during pumping to characterize specific storage and hydraulic conductivity of semi-confining units. J. Hydrol. 281, 3–22. https://doi.org/10.1016/S0022-1694, (03)00197-5.

Butler Jr, J.J., 1988. Pumping tests in nonuniform aquifers—the radially symmetric case. J. Hydrol. 101, 15–30. https://doi.org/10.1016/0022-1694, (88)90025-X.

Cassiani, G., Kabala, Z., Medina Jr, M., 1999. Flowing partially penetrating well: solution to a mixed-type boundary value problem. Adv. Water Resour. 23, 59–68. https://doi.org/10.1016/S0309-1708, (99)00002-0.

Chang, C.C., Chen, C.S., 2002. An integral transform approach for a mixed boundary problem involving a flowing partially penetrating well with infinitesimal well skin. Water Resour. Res. 38. https://doi.org/10.1029/2001WR001091, 7-1-7-.

Chen, C.S., 1984. A reinvestigation of the analytical solution for drawdown distributions in a finite confined aquifer. Water Resour. Res. 20, 1466–1468. https://doi.org/10.1029/WR020i010p01466.

Chen, S., 2019. Three-dimensional analytical poromechanical solutions for an arbitrarily inclined borehole subjected to fluid injection. Proc. R. Soc. London, Ser. A 475, 20180658. https://doi.org/10.1098/rspa.2018.0658.

Cheng, A.-D., 2016. Poroelasticity. Springer.

De Simone, S., Carrera, J., 2017. Analytical solutions to coupled HM problems to highlight the nonlocal nature of aquifer storage. Water Resour. Res. 53, 9580–9599. https://doi.org/10.1002/2017WR020824.

Dejam, M., Hassanzadeh, H., Chen, Z., 2013. Semi-analytical solutions for a partially penetrated well with wellbore storage and skin effects in a double-porosity system with a gas cap. Transp. Porous Media 100, 159–192. https://doi.org/10.1007/s11242-013-0210-6.

Dejam, M., Hassanzadeh, H., Chen, Z., 2017. Pre-Darcy flow in porous media. Water Resour. Res. 53, 8187–8210. https://doi.org/10.1002/2017WR021257.

Ding, L., Wang, Z., Liu, B., Lv, J., Wang, Y., 2019. Borehole stability analysis: a new model considering the effects of anisotropic permeability in bedding formation based on poroelastic theory. J. Nat. Gas Sci. Eng. 69, 102932. https://doi.org/10.1016/j.jngse.2019.102932.

Fan, Z., Eichhubl, P., Gale, J.F., 2016. Geomechanical analysis of fluid injection and seismic fault slip for the Mw4. 8 Timpson, Texas, earthquake sequence. J. Geophys. Res. B 121, 2798–2812. https://doi.org/10.1002/2016JB012821.

Fan, Z., Eichhubl, P., Newell, P., 2019. Basement fault reactivation by fluid injection into sedimentary reservoirs: poroelastic effects. J. Geophys. Res. B 124, 7354–7369. https://doi.org/10.1029/2018JB017062.

Fan, Z., Parashar, R., 2019. Analytical solutions for a wellbore subjected to a non-isothermal fluid flux: implications for optimizing injection rates, fracture re-activation, and EGS hydraulic stimulation. Rock Mech. Rock Eng. 4715–4729. https://doi.org/10.1007/s00603-019-01867-9.

Fan, Z., Parashar, R., Jin, Z.-H., 2020. Impact of convective cooling on pore pressure and stresses around a borehole subjected to a constant flux: implications for hydraulic tests in an EGS reservoir. Interpretation 8, SG13–SG20. https://doi.org/10.1190/int-2019-0180.1.

Feng, Q., Zhan, H., 2016. Integrated aquitard-aquifer flow with a mixed-type well-face boundary and skin effect. Adv. Water Resour. 89, 42–52. https://doi.org/10.1016/j.advwatres.2016.01.003.

Ferroud, A., Rafini, S., Chesnaux, R., 2019. Using flow dimension sequences to interpret non-uniform aquifers with constant-rate pumping-tests: a review. J. Hydrol. 2, 100003. https://doi.org/10.1016/j.hydroa.2018.100003.

Ghassemi, A., Zhou, X., 2011. A three-dimensional thermo-poroelastic model for fracture response to injection/extraction in enhanced geothermal systems. Geothermics 40 (1), 39–49. https://doi.org/10.1016/j.geothermics.2010.12.001.

Green, D., Wang, H., 1990. Specific storage as a poroelastic coefficient. Water Resour. Res. 26, 1631–1637. https://doi.org/10.1029/WR026i007p01631.

Hantush, M.S., 1964. Hydraulics of wells. Adv. Hydrosci. 1, 281–432.

Hsieh, P.A., 1996. Deformation-induced changes in hydraulic head during ground-water withdrawal. Groundwater 34, 1082–1089. https://doi.org/10.1111/j.1745-6584.1996.tb02174.x.

Hsieh, P.A., Cooley, R.L., 1995. Comment on" Horizontal aquifer movement in a theis-theim confined system, by Donald C. Helm. Water Resour. Res. 31, 3107–3111. https://doi.org/10.1029/95WR02713.

Jacob, C.E., 1940. On the flow of water in an elastic artesian aquifer. Eos, Trans. Am. Geophys. Union 21, 574–586. https://doi.org/10.1029/TR021i002p00574.

Koh, J., Roshan, H., Rahman, S.S., 2011. A numerical study on the long-term thermo-poroelastic effects of cold water injection into naturally fractured geothermal reservoirs. Comput. Geotechnics 38 (5), 669–682. https://doi.org/10.1016/j.compgeo.2011.03.007.

Li, N., Wen, Z., Zhan, H., Zhu, Q., 2018. The single-well test dilemma: the skin effect and variable-rate pumping perspective. Hydrogeol. J. 26, 2521–2529. https://doi.org/10.1007/s10040-018-1852-9.

Mathias, S., Butler, A., 2007. Flow to a finite diameter well in a horizontally anisotropic aquifer with wellbore storage. Water Resour. Res. 43. https://doi.org/10.1029/2006WR005839.

Mehrabian, A., Abousleiman, Y.N., 2013. Generalized poroelastic wellbore problem.. Int. J. Numer. Anal. Methods Geomech. 37, 2727–2754. https://doi.org/10.1002/nag.2160.

Moench, A.F., 1997. Flow to a well of finite diameter in a homogeneous, anisotropic water table aquifer. Water Resour. Res. 33, 1397–1407. https://doi.org/10.1029/97WR00651.

Neuzil, C.E., 1986. Groundwater flow in low-permeability environments. Water Resour. Res. 22, 1163–1195. https://doi.org/10.1029/WR022i008p01163.

Novakowski, K.S., 1989. A composite analytical model for analysis of pumping tests affected by well bore storage and finite-thickness skin. Water Resour. Res. 25, 1937–1946. https://doi.org/10.1029/WR025i009p01937.

Papadopulos, I.S., Cooper, H.H., 1967. Drawdown in a well of large diameter. Water Resour. Res. 3, 241–244. https://doi.org/10.1029/WR003i001p00241.

Park, E., Zhan, H., 2002. Hydraulics of a finite-diameter horizontal well with wellbore storage and skin effect. Adv. Water Resour. 25, 389–400. https://doi.org/10.1016/S0309-1708(02)00011-8.

Pasandi, M., Samani, N., Barry, D., 2008. Effect of wellbore storage and finite-thickness skin on flow to a partially penetrating well in a phreatic aquifer. Adv. Water Resour. 31, 383–398. https://doi.org/10.1016/j.advwatres.2007.09.001.

Razminia, K., Razminia, A., Machado, J.T., 2016. Analytical solution of fractional order diffusivity equation with wellbore storage and skin effects. J. Comput. Nonlinear Dyn. 11, 011006. https://doi.org/10.1115/1.4030534.

Razminia, K., Razminia, A., Trujilo, J.J., 2015. Analysis of radial composite systems based on fractal theory and fractional calculus. Signal Process. 107, 378–388. https://doi.org/10.1016/j.sigpro.2014.05.008.

Sneed, M., Brandt, J.T., Solt, M., 2018. In: Land Subsidence Along the California Aqueduct in West-Central San Joaquin Valley, 2003–10. US Geological Survey, California, p. 5144.

Stehfest, H., 1970. Numerical inversion of Laplace transforms. Commun. ACM 13, 47–49. https://doi.org/10.1145/361953.361969.

Theis, C.V., 1935. The relation between the lowering of the piezometric surface and the rate and duration of discharge of a well using ground-water storage. Eos, Trans. Am. Geophys. Union 16, 519–524. https://doi.org/10.1029/TR016i002p00519.

Tsang, C.F., Neretnieks, I., Tsang, Y., 2015. Hydrologic issues associated with nuclear waste repositories. Water Resour. Res. 51, 6923–6972. https://doi.org/10.1002/2015WR017641.

Wang, H.F., 1993. Quasi-static poroelastic parameters in rock and their geophysical applications. Pure Appl. Geophys. 141, 269–286. https://doi.org/10.1007/BF00998332.

Wang, H.F., 2000. Theory of Linear Poroelasticity With Applications to Geomechanics and Hydrogeology. Princeton University Press.

Wu, Y., Liu, J., Elsworth, D., Chen, Z., Connell, L., Pan, Z., 2010. Dual poroelastic response of a coal seam to CO2 injection. Int. J. Greenhouse Gas Control 4 (4), 668–678. https://doi.org/10.1016/j.ijggc.2010.02.004.

Yang, S.Y., Yeh, H.D., Chiu, P.Y., 2006. A closed form solution for constant flux pumping in a well under partial penetration condition. Water Resour. Res. 42. https://doi.org/10.1029/2004WR003889.

Yeh, H.-D., Chang, Y.-C., 2013. Recent advances in modeling of well hydraulics. Adv. Water Resour. 51, 27–51. https://doi.org/10.1016/j.advwatres.2012.03.006.

Yeh, H.-D., Yang, S.-Y., Peng, H.-Y., 2003. A new closed-form solution for a radial two-layer drawdown equation for groundwater under constant-flux pumping in a finite-radius well. Adv. Water Resour. 26, 747–757. https://doi.org/10.1016/S0309-1708(03)00046-0.

Yin, S., Dusseault, M.B., Rothenburg, L., 2007. Analytical and numerical analysis of pressure drawdown in a poroelastic reservoir with complete overburden effect considered. Adv. Water Resour. 30, 1160–1167. https://doi.org/10.1016/j.advwatres.2006.10.008.